Scientific Reports

https://doi.org/10.1038/s41598-026-61096-3

Article in Press

Effects of grinding penetration depth and abrasive grain spacing on atomic interactions and material removal mechanisms in silicon during ultrasonic vibration-assisted grinding: a molecular dynamics study

Received: 11 May 2026

Accepted: 2 July 2026

Published online: 19 July 2026

Cite this article as: Singh N.S.S., Hassan W.H., Alaloosi W. *et al.* Effects of grinding penetration depth and abrasive grain spacing on atomic interactions and material removal mechanisms in silicon during ultrasonic vibration-assisted grinding: a molecular dynamics study. *Sci Rep* (2026). https://doi.org/10.1038/s41598-026-61096-3

Narinderjit Singh Sawaran Singh, Waqed H. Hassan, Waleed Alaloosi, Watfaa Khayri Younis, Banaz Shahab Haji, Mahmut Taner, Soheil Salahshour & S. Mohammad Sajadi

Effects of Grinding Penetration Depth and Abrasive Grain Spacing on Atomic Interactions and Material Removal Mechanisms in Silicon during Ultrasonic Vibration-Assisted Grinding: A Molecular Dynamics Study

1. Narinderjit Singh Sawaran Singh
Faculty of Data Science and Information Technology, INTI International University, Persiaran Perdana BBN, Putra Nilai, Nilai 71800, Malaysia.
narinderjits.sawaran@newinti.edu

2. Waqed H. Hassan
Advanced Technical College, University of Warith Al-Anbiyaa, Karbala, Iraq.
waqed.hammed@uowa.edu.iq

3. Waleed Alaloosi
Department of Medical Instruments Engineering Techniques, College of Engineering, University of Al Maarif, Al Anbar,31001, Iraq.
waleed.muwafaq@uoa.edu.iq

4. Watfaa Khayri Younis
Al-Amarah University College, Maysan, Iraq.

5. Banaz Shahab Haji
Medical Radiology Imaging Department, College of Health Sciences,
Lebanese French University (LFU), Kurdistan Region, Erbil, Iraq.
banaz.shahab@lfu.edu.krd

6- Mahmut Taner
Faculty of Engineering and Architecture, Istanbul Gelisim University, Istanbul, Türkiye
mtaner340@gmail.com

7- Soheil Salahshour
Faculty of Engineering and Natural Sciences, Istanbul Okan University, Istanbul, Turkey
Faculty of Engineering and Natural Sciences, Bahcesehir University, Istanbul, Turkey
Research Center of Applied Mathematics, Khazar University, Baku, Azerbaijan
Faculty of Science and Letters, Piri Reis University, Tuzla, Istanbul, Turkey
soheil.salahshour1361@gmail.com

8- S. Mohammad Sajadi*
Department of Chemistry, Payam e Noor University, Saqqez Branch, Saqqez, Kurdistan, Iran.
sajadhamedi13661366@gmail.com

***Corresponding Author: S. Mohammad Sajadi;** sajadhamedi13661366@gmail.com

Abstract
Grinding is an important finishing process for hard, brittle materials like silicon, where atomic-level finishing is critical for semiconductor and microelectronic applications. Ultrasonic vibration-assisted grinding has been shown to enhance grinding efficiency beyond conventional methods, but several of its atomic-level mechanisms remain incompletely understood. The interaction among the following was investigated in this study: mean abrasive grain spacing, grinding penetration depth, and abrasive grain physical properties. Atomic interactions and behaviors of the grinding process were modeled using molecular dynamics. An equilibration of 10 ns was first set up, during which extrinsic variables were manipulated to produce an equivalent environment, allowing the sample to evolve independently. This equilibration step was essential to achieve stabilization, since the potential and kinetic energies were −4.69 eV and 0.02 eV, respectively. It was observed that changing the grinding penetration depth from 10 Å to 16 Å significantly affected important atomic parameters: the number of detached atoms increased from 2231 to 2495, whereas the maximum stress rose from 10.26 to 12.27 GPa. This result was remarkable because it indicated strong stress localization and enhanced atomic bond breakage at deeper penetration depths, revealing the onset of severe atomic deformation. The highest force of the system increased from 606.67 to 725.05 GPa·nm². Increasing the mean abrasive grain spacing between abrasive grains from 31 to 45 Å resulted in a lower number of dissociative atoms (2231 → 2154) and a shallower penetration depth (10.75 → 10.29 Å). The maximum stress and, in turn, the force were found to decrease uniformly from 10.26 to 9.89 GPa and from 584.80 GPa·nm² to 560.80 GPa·nm², respectively.

Keywords: Grinding penetration depth, Molecular Dynamic Simulation, Physical properties, Maximum Stress**.** manufacturing investment

Table of abbreviations

Pulsed laser-assisted ultrasonic grinding	PL-UAG
Molecular Dynamics Simulations	MDS
Radial Distribution Function	RDF
Maximum	Max
Density Functional Theory	DFT
Ultrasonic-Assisted Grinding	UAG
Ultrasonic Vibration-Assisted Grinding	UVAG

1. Introduction

Grinding and vibration-assisted processing technologies are widely employed in modern manufacturing because they improve material removal efficiency, machining precision, and surface quality. Beyond precision machining, vibration-assisted techniques have also been applied in mineral processing, extractive metallurgy, and materials synthesis to enhance fragmentation, mass transfer, and process efficiency [1-3]. The common principle underlying these applications is that externally applied mechanical or acoustic energy modifies the

deformation and fracture behavior of the material. Building on this concept, ultrasonic vibration-assisted grinding (UVAG) has emerged as an effective machining technology for hard and brittle materials, where intermittent abrasive-workpiece contact can significantly improve grinding performance compared with conventional grinding [4, 5]. Among advanced precision-machining technologies, ultrasonic vibration-assisted grinding (UVAG) has attracted considerable attention for processing hard and brittle materials, such as silicon, silicon carbide, ceramics, and advanced composites. By superimposing high-frequency and low-amplitude vibration on either the grinding tool or the workpiece, the contact state changed from continuous sliding to intermittent impact and sliding. This modified contact condition reduced grinding force, improved chip evacuation, suppressed heat accumulation, and enhanced surface integrity compared with conventional grinding [6-9]. However, the effectiveness of ultrasonic vibration-assisted grinding was strongly influenced by the interaction between vibration kinematics and abrasive-workpiece contact geometry, making the underlying deformation and material-removal mechanisms highly dependent on nanoscale contact conditions.

Although experimental and continuum-scale investigations provided valuable information regarding grinding force, surface quality, and process efficiency, they cannot directly resolve atomic-scale deformation and material-removal mechanisms. Molecular dynamics (MD) simulation, therefore, became an important tool for studying nanoscale grinding, enabling direct observation of bond breaking, atomic displacement, stress localization, phase transformation, amorphization, and defect evolution during abrasive interaction. Previous MD studies clarified several isolated aspects of nanoscale grinding. For example, Liu et al. [10] and Li et al. [11] investigated the influence of grinding depth and demonstrated that increasing penetration depth intensified atomic displacement, grinding force, subsurface damage, and burr formation in

silicon and silicon carbide systems. Chen [12] and Li et al. [13] examined lubrication layers and surface-film effects and reported that interfacial conditions strongly affected tangential force, energy dissipation, and damage accumulation during nanogrinding. Additional studies examined the effects of grinding parameters, abrasive motion, surface roughness, and process conditions on material removal and the evolution of subsurface damage in silicon-based materials [14-20]. More recently, MD simulations were extended to ultrasonic vibration-assisted grinding. Huang et al. [21] demonstrated that vibration direction significantly influenced impact characteristics, stress redistribution, dislocation activity, and microstructural evolution during ultrasonic grinding. These findings confirmed that ultrasonic excitation fundamentally altered the deformation pathway compared with conventional grinding. Nevertheless, most existing atomistic investigations remained parameter-isolated, focusing primarily on individual variables, such as grinding depth, lubrication condition, vibration direction, abrasive geometry, or boundary condition. Although such studies provided valuable mechanistic insights, they did not fully capture the coupled contact mechanics that occurred in realistic multi-abrasive grinding environments.

Abrasive grain spacing was another important geometric parameter that received considerably less attention than grinding depth. In practical grinding processes, multiple abrasive grains simultaneously interact with the workpiece surface. Consequently, the stress field, pile-up region, thermal disturbance zone, and defect structure generated by one abrasive grain can interact with those generated by neighboring grains. The spacing between adjacent abrasives, therefore, governs whether local deformation zones remain independent or overlap, directly influencing atomic detachment, stress concentration, subsurface damage, force fluctuations, and surface integrity. Understanding this interaction was particularly important under ultrasonic

vibration-assisted conditions, where intermittent contact and cyclic loading continuously modified the evolution of neighboring stress fields.

Only a limited number of MD studies considered multi-abrasive grinding. For example, Karkalos et al. [22] investigated the influence of abrasive-grain spacing and rake angle on grinding force, chip formation, temperature evolution, and subsurface damage during nanogrinding, demonstrating that abrasive spacing significantly affected interactions among neighboring deformation zones. However, these studies were conducted under conventional nanogrinding conditions and did not examine the coupled influence of abrasive spacing and grinding penetration depth under ultrasonic vibration-assisted grinding of monocrystalline silicon. Similarly, existing ultrasonic vibration-assisted grinding simulations have primarily focused on vibration direction, vibration mode, or force reduction, while the combined roles of penetration depth and abrasive spacing in controlling atomic-scale stress-field interactions, defect evolution, and material-removal behavior remain insufficiently understood.

To further clarify the current state of research and highlight the specific gap addressed in this work, Table 1 summarizes representative studies on nanoscale grinding and ultrasonic vibration-assisted grinding, including the primary parameters investigated, key findings, and remaining limitations. The comparison demonstrates that previous investigations mainly focused on isolated parameters, such as grinding depth, lubrication conditions, vibration direction, or abrasive spacing, whereas the coupled influence of grinding penetration depth and abrasive grain spacing under ultrasonic vibration-assisted grinding of monocrystalline silicon remains largely unexplored.

Table 1. Comparison of representative MD studies on nanoscale grinding and ultrasonic vibration-assisted grinding, highlighting the investigated parameters, key findings, existing limitations, and the research gap addressed by the present study.

Study	Material / Method	Main parameter investigated	Main contribution	Limitation/gap	Relevance to the present work
Liu et al. [10]	Single-crystal SiC / MD nanogrinding	Grinding depth	Demonstrated that larger grinding depth increases atomic displacement, force, and defect formation.	Single-parameter study; no multi-abrasive spacing or ultrasonic vibration.	Provides depth-related baseline for brittle-material nanogrinding.
Li et al. [11]	Monocrystalline Si / MD nanogrinding	Grinding depth/burr formation	Clarified the relation between grinding depth, force evolution, subsurface defect formation, and burr generation in silicon.	Did not consider abrasive spacing or ultrasonic vibration.	Directly relevant to depth-dependent silicon removal.
Chen [12]	TiAl alloy / MD nanogrinding	Humidity/water layer thickness	Showed that the lubrication condition affects the grinding force, especially the tangential force and interfacial energy dissipation.	Focused on boundary/lubrication condition rather than grinding depth or abrasive spacing.	Supports the idea that local boundary conditions modify atomic-scale grinding response.
Li et al. [13]	Single-crystal Si / MD nanogrinding	Surface films	Showed how surface films modify nanometric grinding response.	The study itself notes that single-abrasive models cannot fully represent coupled multi-abrasive grinding.	Helps justify the need for multi-abrasive modeling.
Wu et al. [15]	Silicon wafer / MD nanogrinding	Surface roughness and grinding depth	Showed that grinding depth and surface roughness affect the removal regime, temperature, von Mises stress, force, and damage.	Single-abrasive configuration; no abrasive spacing or UVAG coupling.	Supports the importance of depth in silicon nanogrinding.
Zhao et al. [16]	Single-crystal Si / MD nanogrinding	Grinding parameters such as depth, speed, and temperature	Linked grinding parameters to phase transformation, residual stress, and subsurface damage.	Parameter effects were not coupled with abrasive spacing under ultrasonic vibration.	Provides silicon-specific MD evidence for parameter-dependent damage.
Huang et al. [21]	Polycrystalline Fe / MD UVAG	Vibration direction	Showed that vibration direction changes force response, stress redistribution, dislocation activity, and microstructural evolution.	Focused on vibration mode; did not examine grinding depth–abrasive spacing coupling.	Supports the role of ultrasonic kinematics in atomic-scale deformation.
Karkalos et al. [22]	Workpiece material / multi-abrasive MD nanogrinding	Abrasive spacing and rake angle	Developed a multi-abrasive MD model and showed that abrasive spacing affects chip formation, force, temperature, and subsurface damage.	Conventional nanogrinding; no ultrasonic vibration and no systematic coupling with penetration depth in silicon.	Key reference showing that abrasive spacing is important in multi-abrasive grinding.
Present study	Monocrystalline Si / multi-abrasive MD UVAG	Grinding depth and abrasive grain spacing	Quantifies the independent and coupled effects of grinding penetration depth and abrasive grain spacing on atomic detachment, stress localization, force evolution, and subsurface damage during UVAG.	—	Addresses the coupled influence of penetration depth and abrasive spacing in multi-abrasive UVAG of monocrystalline silicon.

To address this gap, the present study developed a multi-abrasive MD model of ultrasonic vibration-assisted grinding of monocrystalline silicon. Grinding penetration depth and abrasive grain spacing were independently varied to systematically investigate their individual and coupled influences on atomic detachment, grinding force, von Mises stress, displacement fields, dislocation activity, and subsurface structural transformation. Accordingly, the novelty of the present work lies in establishing an atomistic framework that resolves the coupled effects of penetration depth and abrasive spacing under ultrasonic vibration-assisted grinding conditions. By simultaneously considering these two geometric parameters within a multi-abrasive silicon grinding model, the study clarified how stress-field interaction, defect evolution, and atomic-scale deformation collectively governed material-removal behavior and subsurface damage formation.

2. Numerical method

2.1.Simulation model and geometric configuration

The ultrasonic vibration-assisted grinding process was investigated using molecular dynamics simulations performed in the LAMMPS package. The simulation model consisted of a monocrystalline silicon substrate with dimensions of approximately 160 × 80 × 73 $Å^3$, and eight octahedral diamond abrasive grains positioned above the workpiece surface, as shown in Fig. 1. The complete atomistic system contained 22,319 atoms. Periodic boundary conditions were applied along with x and y directions to minimize finite-size effects, while a non-periodic boundary condition was employed in the z direction to allow free-surface deformation and material removal. The lower ten atomic layers of the silicon substrate were fixed throughout the simulation to prevent rigid-body motion and improve numerical stability. The remaining silicon

atoms were fully mobile and evolved according to Newtonian dynamics during equilibration and grinding. The abrasive grain spacing, one of the principal variables investigated in this work, was defined as the center-to-center distance between adjacent diamond abrasive grains projected onto the workpiece surface. The spacing values varied from 31 Å to 45 Å. This parameter differed from the grinding penetration depth, which described the vertical engagement of abrasive grains into the silicon substrate. The selected spacing range was intended to investigate the interaction and overlap of neighboring stress fields generated during multi-abrasive grinding.

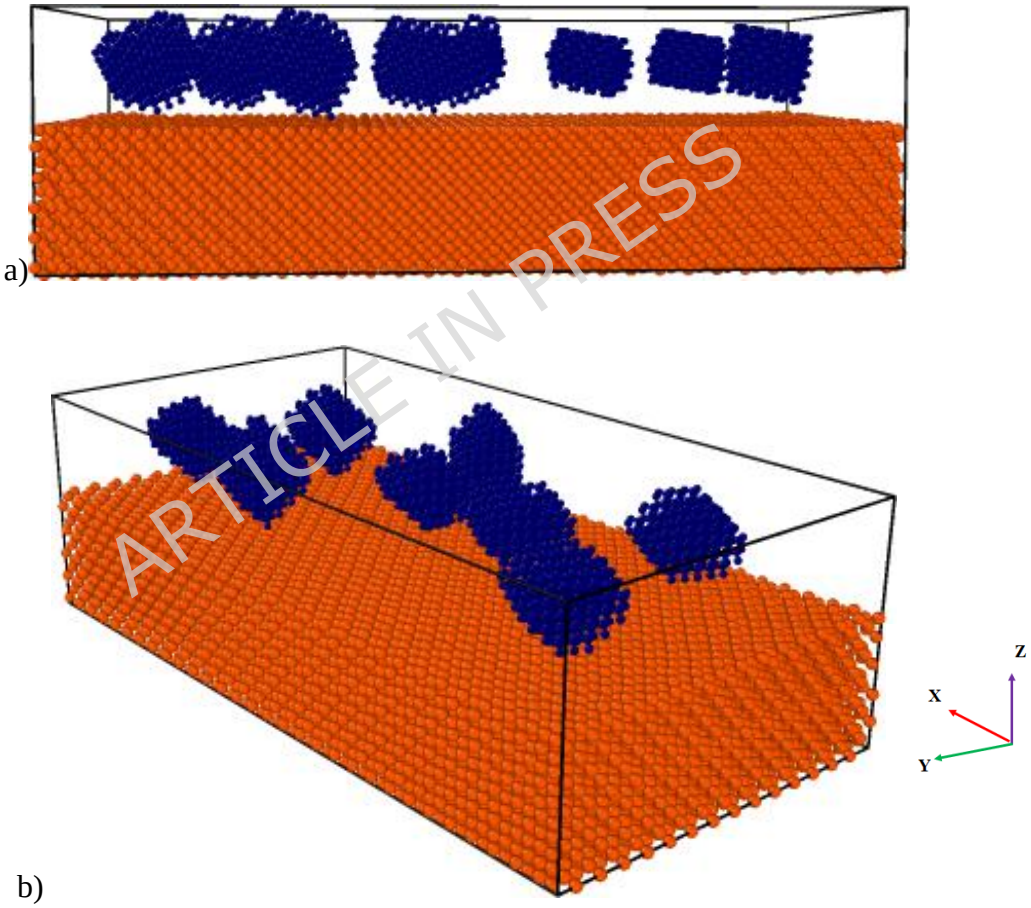

Fig.1. A schematic of the present simulation box from a) front and b) perspective views.

2.2.Interatomic potential and force-field description

All atomic interactions were modeled using the Tersoff bond-order potential with the SiC parameterization [23].

$$E = \frac{1}{2}\sum_{i}\sum_{i \neq j} U_{ij} \tag{1}$$

$$U_{ij} = f_C\left(r_{ij}\right)\left[f_R\left(r_{ij}\right) + b_{ij} f_A\left(r_{ij}\right)\right] \tag{2}$$

In LAMMPS, the Tersoff potential was implemented using the command (pair_style tersoff, pair_coeff * * SiC.tersoff C Si) where atom type 1 corresponded to carbon atoms in the diamond abrasive grains and atom type 2 corresponded to silicon atoms in the workpiece. Consequently, the same parameterization was used to describe Si–Si, C–C, and Si–C interactions throughout the simulation domain. The Tersoff potential was selected because it accurately represented covalent materials undergoing mechanical deformation. Unlike pairwise interaction models, the Tersoff formalism accounts for local atomic coordination, bond-order dependence, angular interactions, and bond-breaking and bond-forming processes. These characteristics were essential for simulating silicon grinding, where material removal was governed by stress-induced bond rupture, amorphization, phase transformation, and defect generation. The diamond abrasive grains were modeled as rigid bodies to preserve their geometric integrity during grinding. This assumption restricted abrasive deformation and wear but did not eliminate abrasive-workpiece interactions. The Si–C interactions remained fully active throughout the simulation, enabling realistic stress transfer, atomic detachment, defect formation, and material removal at the grinding interface. Therefore, the present work focused on the deformation behavior and subsurface damage evolution of the silicon workpiece rather than abrasive wear or abrasive fracture.

2.3.Energy minimization and equilibration procedure

Before grinding, the initial atomic configuration was subjected to conjugate-gradient energy minimization to eliminate unfavorable atomic overlaps and reduce the system potential energy. Following minimization, a short stabilization stage was performed using the nve/limit integration scheme to suppress excessive atomic displacement caused by residual local stresses. Subsequently, a thermal treatment procedure was performed using a Langevin thermostat with a damping parameter of 0.01 ps. The thermal schedule consisted of heating the system from 0 K to 800 K for 100 ps, cooling it from 800 K to 300 K for 100 ps, and maintaining it at 300 K for an additional 100 ps, resulting in a total thermal-conditioning duration of 300 ps. After thermal treatment, the system was equilibrated under the canonical (NVT) ensemble at 300 K for 10 ns to achieve thermal and structural relaxation before mechanical loading.

The attainment of equilibrium was evaluated through the convergence of kinetic energy, total energy, temperature, and root-mean-square displacement (RMSD), which were widely used indicators of thermodynamic and structural stability in molecular dynamics simulations [24-31]. The evolution of kinetic energy and total energy during equilibration is presented in Fig. 2(a,b), while the convergence of temperature and RMSD is shown in Fig. 3(a,b). The convergence of these observables, together with the absence of systematic energy drift, confirmed that the system reached thermodynamic and structural equilibrium before the grinding simulation was initiated.

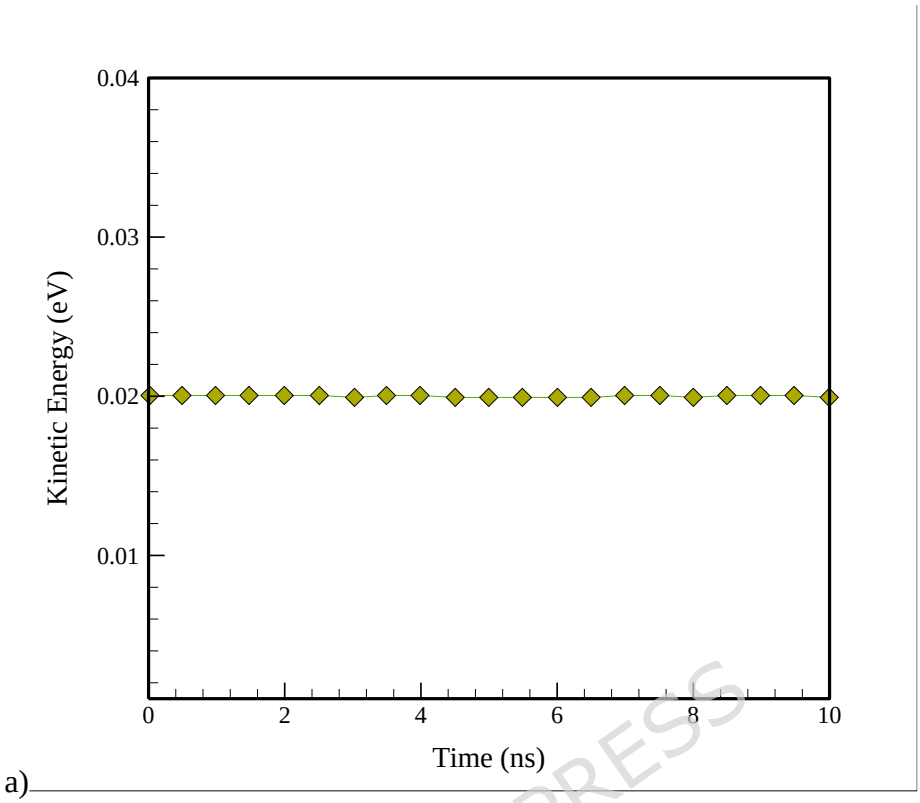

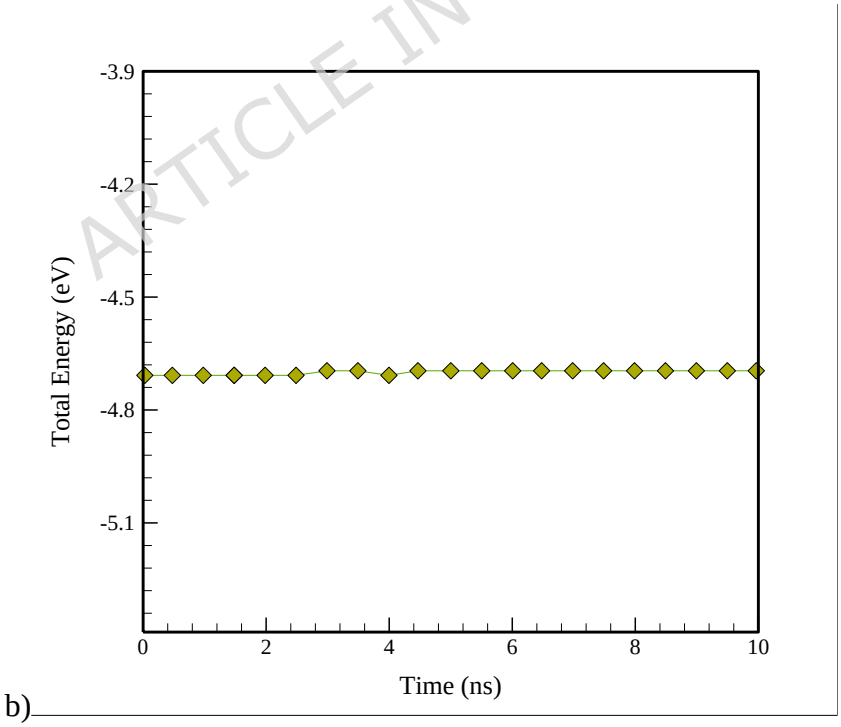

Fig. 2. Variation of a) kinetic and b) total energy for simulation time during the equilibration phase of the sample under the defined initial conditions.

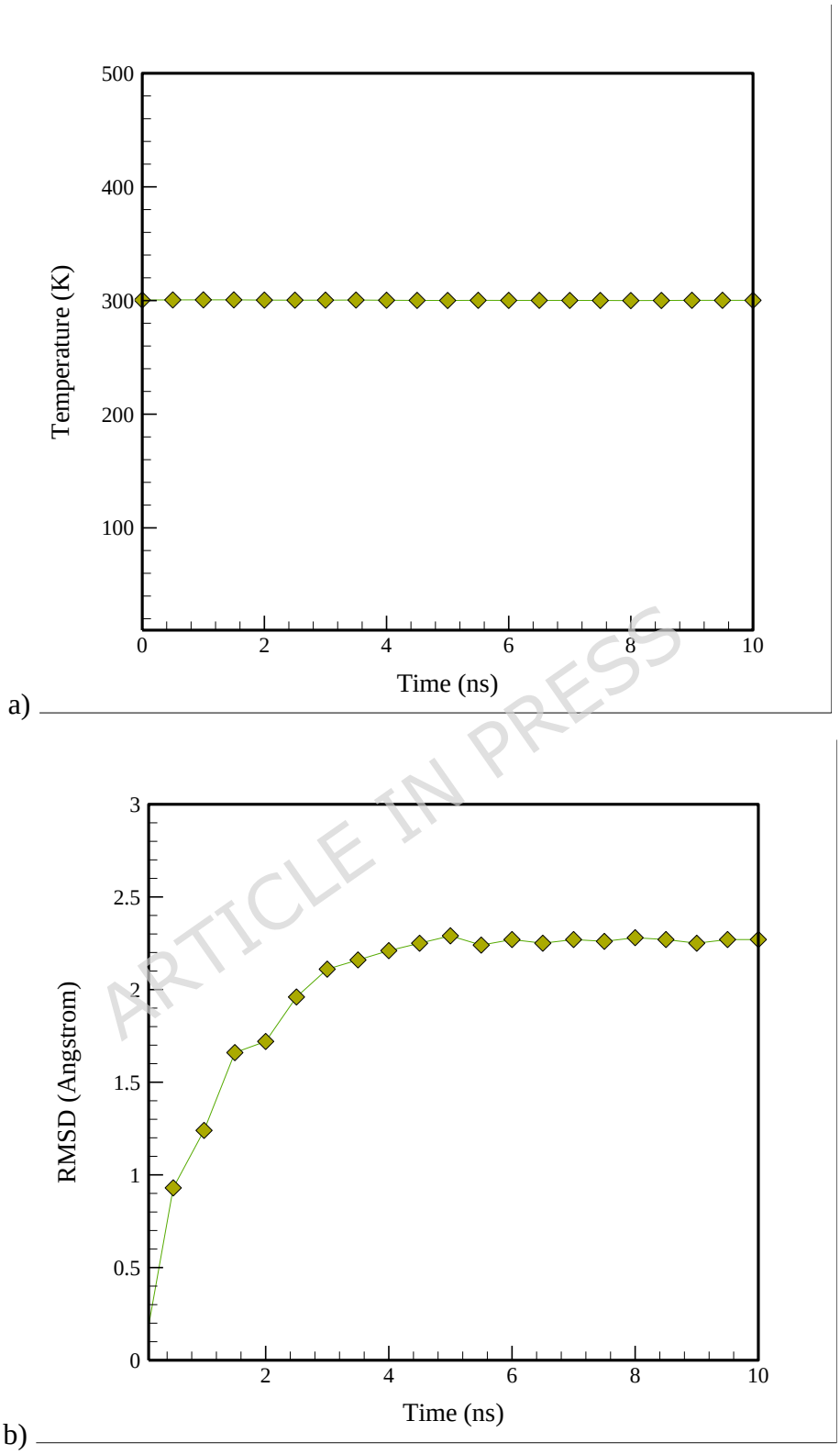

Fig.3. The time variation of a) temperature and b) RMSD parameter in equilibrium phase simulation of pristine atomic structure.

2.4.Ultrasonic vibration-assisted grinding implementation

Following equilibration, the thermostat was removed, and the grinding stage was performed under the microcanonical (NVE) ensemble to avoid artificial damping of contact-induced atomic motion. A time step of 0.1 fs was used throughout all simulations. The grinding penetration depth was controlled by incrementally displacing the abrasive grains along with the negative z direction. The penetration depth was varied by incrementally translating the abrasive group along with the negative z direction using the LAMMPS command displace_atoms D move 0 0 −0.9 units box, thereby increasing the vertical engagement between the abrasive grains and the silicon substrate. This procedure increased the vertical engagement between the abrasive grains and the silicon substrate. The grinding motion was then imposed through prescribed displacements applied to the abrasive group ($Dx = 0.8t$, $Dy = 0.09t + 3\sin(0.0523t)$, $Dz = -|0.005t + \sin(0.0523t)|$), where Dx, Dy, and Dz represent displacement components in Å and t denotes simulation time in ps. The linear terms described the translational grinding motion, whereas the sinusoidal terms introduced ultrasonic oscillation. The vibration amplitudes were 3 Å in the y direction and 1 Å in the z direction. The angular frequency $\omega = 0.0523$ rad·ps^{-1} corresponded to approximately 8.3 GHz.

Because MD simulations are inherently limited to nanosecond time scales, reproducing cyclic ultrasonic contact within a computationally feasible simulation requires GHz-scale excitation frequencies to generate sufficient vibration cycles and intermittent contact events. This approach has been widely adopted in atomistic simulations of ultrasonic vibration-assisted grinding because it enables the essential physical mechanisms of cyclic loading, including intermittent impact, stress redistribution, and defect evolution, to be captured within accessible simulation times rather than to reproduce the absolute industrial ultrasonic frequency [21, 32]. Technically,

the GHz frequency was an atomistic computational analogue chosen to mimic the cyclic kinematics and contact intermittency of kHz-range ultrasonic-assisted grinding within MD timescales, and quantify the expected systematic differences: higher frequency produced correspondingly higher instantaneous strain rates and may enhance inertial and rate-dependent phenomena (e.g., elevated local stress peaks, faster defect nucleation) compared with kHz experiments, so direct quantitative transfer of magnitudes (force peaks, absolute damage depths) to macroscopic UAG should be done with caution. To preserve the study's relevance, the study emphasized current conclusions focused on relative trends (effects of penetration depth and inter-grain spacing, mechanisms of stress-field interaction, and qualitative changes in defect evolution under cyclic loading) that were robust to the frequency scaling inherent to the MD approach.

2.5.Structural validation and RDF analysis

The radial distribution function (RDF) was employed to verify the structural stability and atomic ordering of the equilibrated silicon substrate. RDF analysis provided information regarding short-range and long-range atomic arrangements and was commonly used to distinguish crystalline, amorphous, and liquid phases. The RDF obtained after equilibration exhibited pronounced peaks corresponding to the characteristic crystalline structure of silicon, indicating the preservation of long-range atomic order (See Fig. 4). The close agreement between the calculated RDF and previously reported experimental and computational data confirmed the validity of the adopted force field and equilibration procedure [33, 34]. The RDF comparison also confirmed that the crystalline structure of silicon was preserved after equilibration and before the grinding stage.

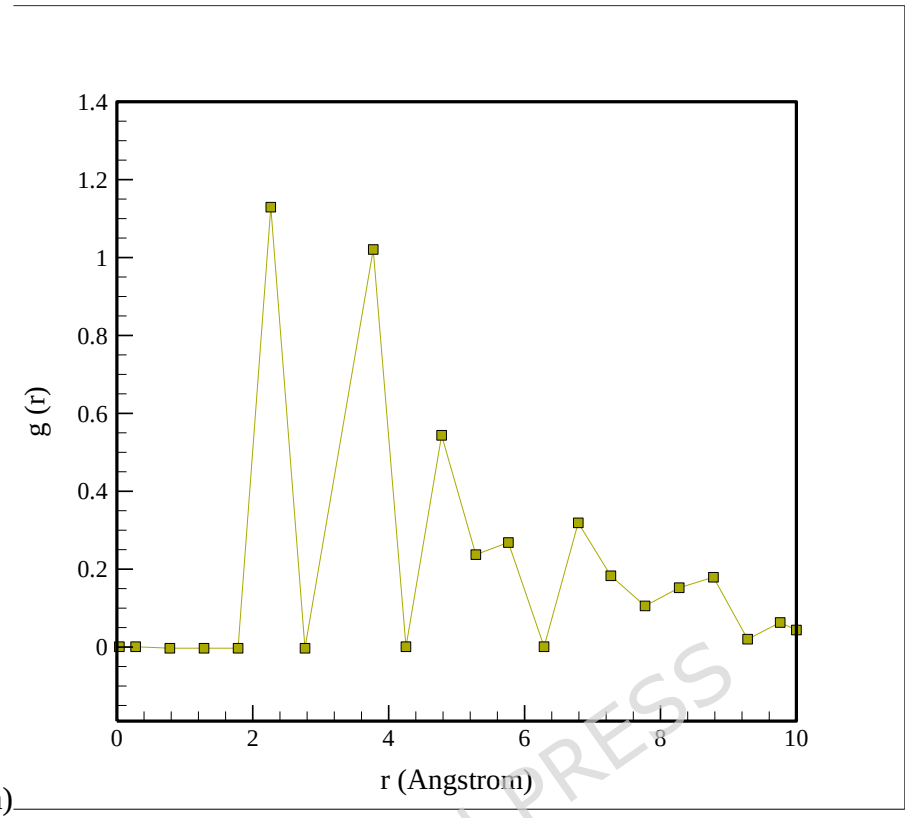

a)

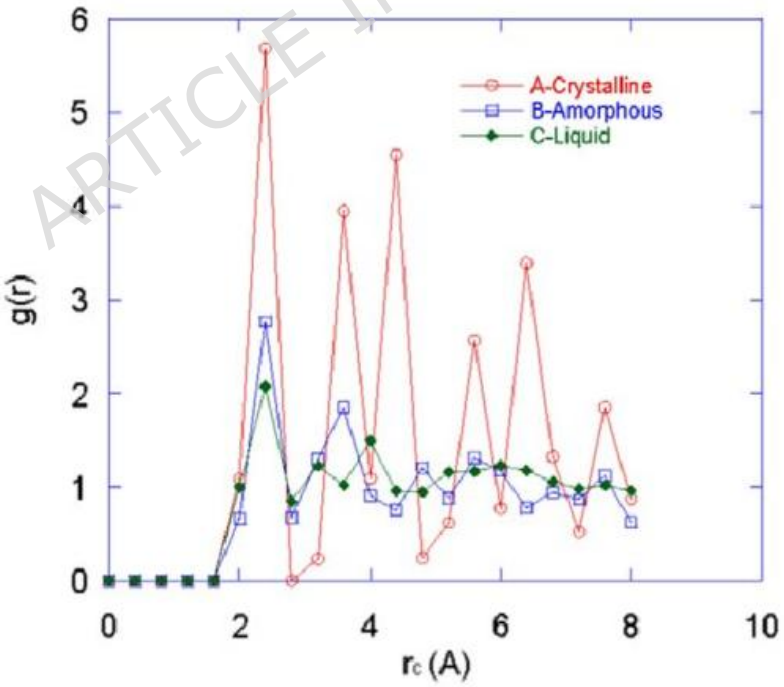

b)

Fig.4. The RDF derived from the silicon sample following the attainment of thermodynamic equilibrium within the simulation box (a) the present study (b) reference [33].

2.6. Stress and defect analysis

The local atomic stress state was calculated using the LAMMPS compute stress/atom command. The resulting stress tensor components were used to evaluate von Mises stress distributions and identify regions of stress concentration generated during abrasive–workpiece interaction. Subsurface structural evolution was further characterized through defect and dislocation analyses. Defects and dislocation-like structures were identified using the Dislocation Extraction Algorithm implemented in OVITO. These analyses provided information regarding stress localization, defect accumulation, atomic detachment, and subsurface damage development as functions of grinding penetration depth and abrasive grain spacing.

3. Results and discussion

Following the grinding process, the atomic structure of the silicon substrate showed significant disorder compared with its equilibrated crystalline configuration. This evolution is evident from the RDF shown in Fig. 5, where the reduction in peak intensity and the broadening of neighboring peaks indicate the loss of long-range crystalline order and the development of a more disordered atomic arrangement relative to the pristine structure presented in Fig. 4. The coordination-number analysis further reveals substantial local bond rearrangement caused by abrasive-induced deformation, indicating that many silicon atoms departed from their ideal crystalline coordination environment. This interpretation is further supported by the amorphous atom fraction, which increased markedly from 20.30% before grinding to 80.10% after grinding. Collectively, these structural descriptors indicate that ultrasonic vibration-assisted grinding promotes extensive amorphization and structural disorder in the subsurface region.

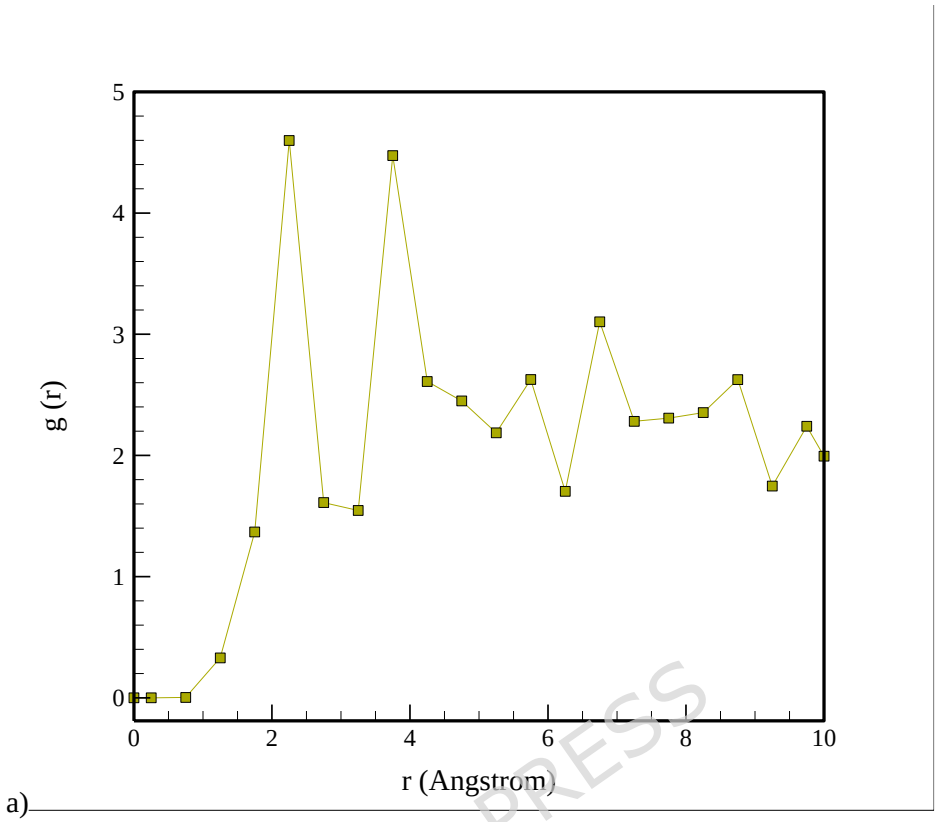

a)

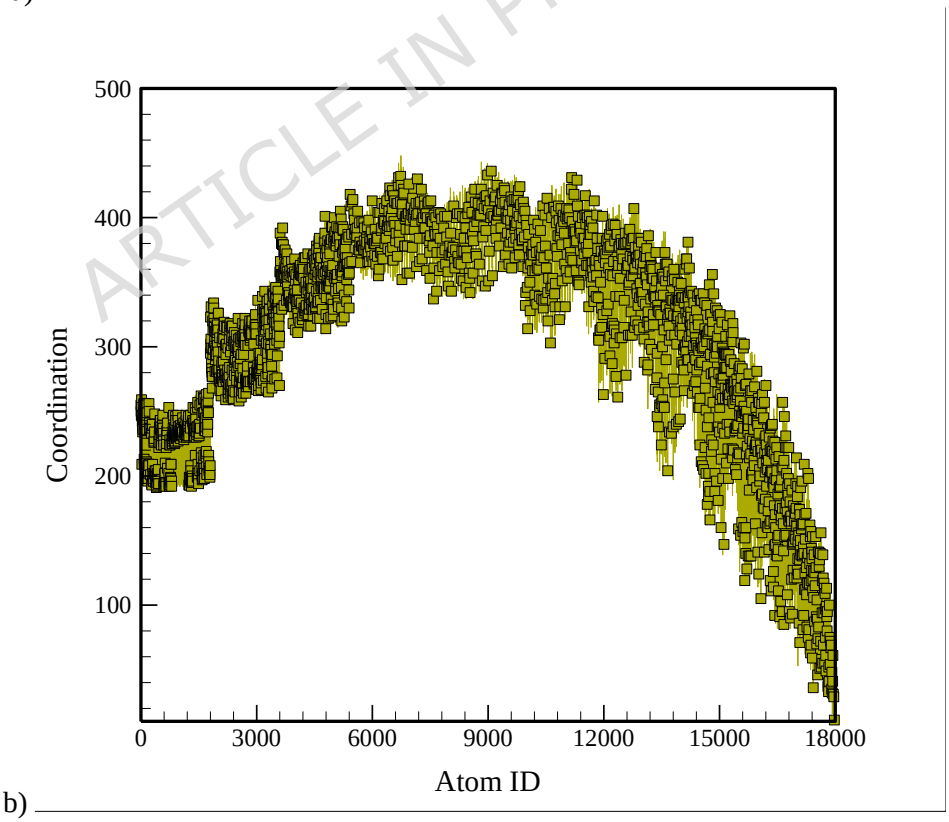

b)

Fig.5. a) RDF and b) coordination outputs of pristine Si substrate after the grinding process occur inside them.

At this stage, the influence of grinding penetration depth on the structural evolution of the silicon substrate was investigated. Fig. 6 presents the atomic configurations obtained at penetration depths of 10, 12, 14, and 16 Å. As the penetration depth increased, the extent of deformation beneath the abrasive trajectories increased. At a depth of 10 Å, the structural disturbance remained relatively localized near the contact regions, indicating limited subsurface deformation. Increasing the penetration depth to 12 and 14 Å enlarged the plastically affected zone and promoted greater atomic displacement around the abrasive-workpiece interface. This behavior indicated that deeper penetration increased the interaction volume between the abrasive grains and the substrate, thereby intensifying local stress concentration and bond distortion. At the maximum penetration depth of 16 Å, the deformation region extends further into the substrate and becomes more interconnected among neighboring abrasive contacts. The larger contact volume increased the compressive and shear stresses on the silicon lattice, leading to greater structural disorder and instability. Consequently, more atoms were displaced from their equilibrium lattice positions, facilitating the initiation and growth of subsurface defects. These observations suggested that the increase in material removal at deeper penetration depths was not solely a geometric consequence of greater engagement but also resulted from intensified stress localization and progressive degradation of the crystalline structure.

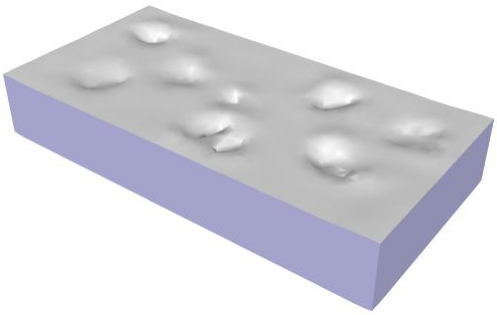

(a)

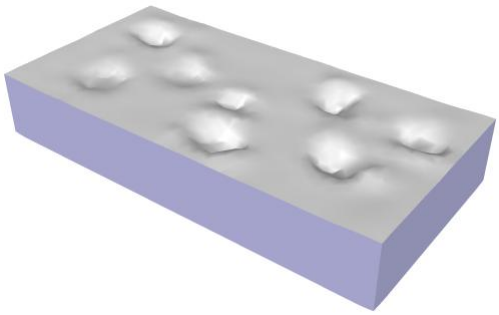

(b)

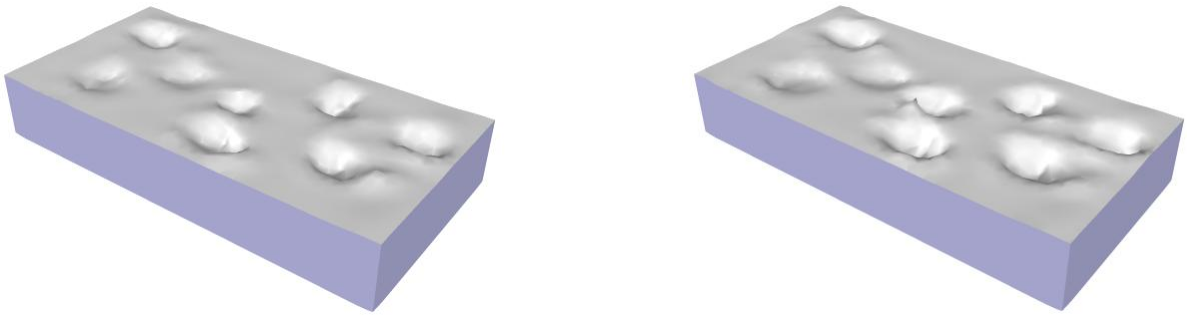

(c) (d)

Fig.6. The changes in atomic structure simulated during the grinding process examined in this study at different depths: a) 10, b) 12, c) 14, and d) 16 **Å**.

The temporal evolution of crystal structure shown in Fig. 7 provides further insight into the underlying deformation mechanism. During the initial stages of grinding, the silicon lattice largely preserved its ordered crystalline arrangement. As the simulation progressed, defect-rich regions gradually emerged beneath the abrasive contact zones and expanded throughout the deformed region. The increasing population of distorted atoms indicated the accumulation of irreversible plastic deformation and local structural disorder. Similar behavior was reported in previous molecular dynamics investigations of silicon grinding, where severe compressive loading promoted defect accumulation, crack initiation, and pressure-induced structural transformations within the subsurface region [18, 19, 35]. The combined observations from Figs. 6 and 7 demonstrate that penetration depth directly influenced the evolution of subsurface damage by governing the magnitude and spatial distribution of stress within the silicon substrate. Higher penetration depths generated larger deformation volumes, accelerated defect accumulation, and reduced lattice stability, thereby facilitating atomic detachment and material removal. Therefore, the observed increase in removed atoms and mechanical response at greater penetration depths originated from a coupled microstructural mechanism involving stress concentration, structural disorder, and the progressive development of subsurface damage, rather

than simply from increased abrasive penetration.

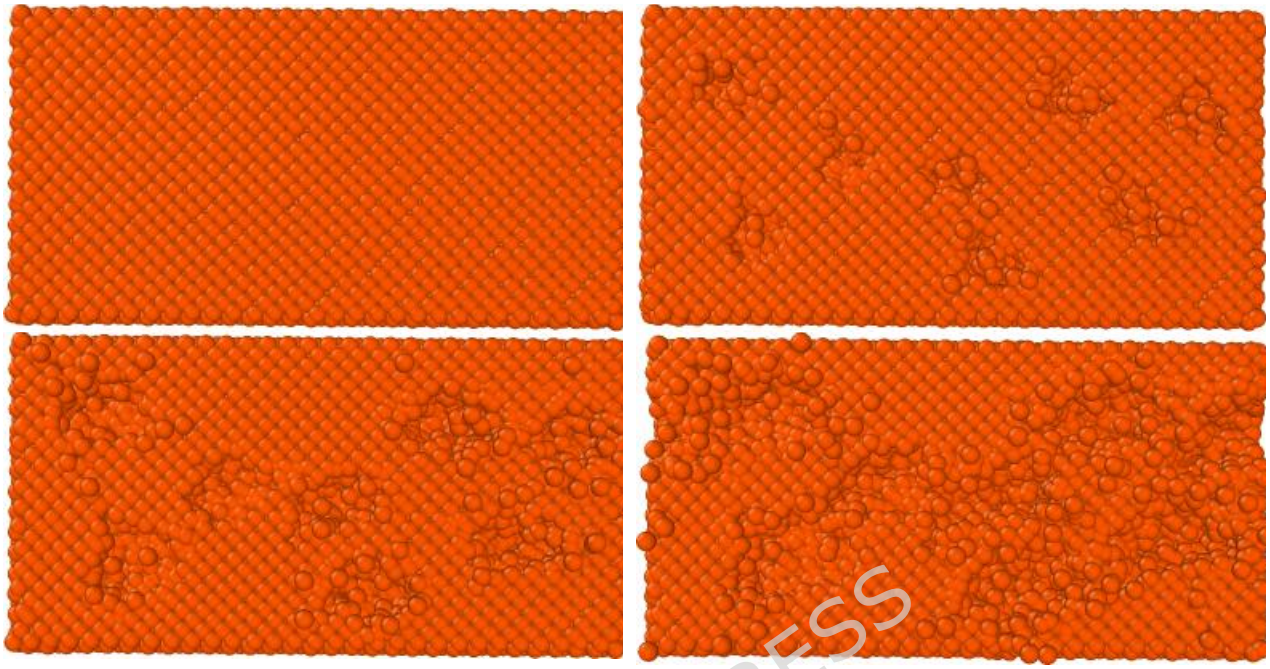

Fig.7. Time evolution of the silicon crystal structure during ultrasonic vibration-assisted grinding, illustrating the progressive formation of defect-rich and structurally disordered regions beneath the abrasive contact zone.

The influence of abrasive grain spacing on the grinding response was subsequently investigated. In the present study, abrasive grain spacing was defined as the center-to-center distance between adjacent abrasive grains projected onto the silicon surface. Four spacing values, namely 31 Å, 35 Å, 40 Å, and 45 Å, were considered to evaluate how neighboring abrasive contacts interacted during multi-abrasive ultrasonic vibration-assisted grinding. Fig. 8 presents the atomic configurations obtained at different abrasive grain spacings. At the smallest spacing of 31 Å, the deformation zones generated by neighboring abrasive grains were closely spaced, leading to significant interaction among local stress fields. As the spacing increased to 35 Å and 40 Å, the overlap between neighboring deformation regions gradually decreased, leading to a more localized distribution of stress and atomic displacement beneath individual abrasive contacts. At the largest spacing of 45 Å, the deformation zones became increasingly separated, and the

interaction among neighboring abrasive-induced stress fields was substantially reduced.

This behavior suggested that abrasive grain spacing influenced material removal through a stress-field interaction mechanism. When abrasive grains were closely spaced, neighboring stress concentrations can interact and reinforce one another, promoting larger deformation regions and more extensive subsurface structural disturbance. In contrast, larger spacing values reduced the degree of stress-field overlap, thereby limiting the propagation of deformation between adjacent abrasive contacts. Consequently, the observed differences in atomic detachment, stress evolution, and defect accumulation were associated not only with individual abrasive action but also with collective interactions among neighboring abrasive grains. Therefore, abrasive grain spacing acted as a governing geometric parameter controlling the extent of stress-field superposition and subsurface damage evolution during multi-abrasive grinding. The results indicated that variations in spacing modified the coupling between neighboring deformation zones, ultimately affecting the material-removal behavior of the silicon substrate.

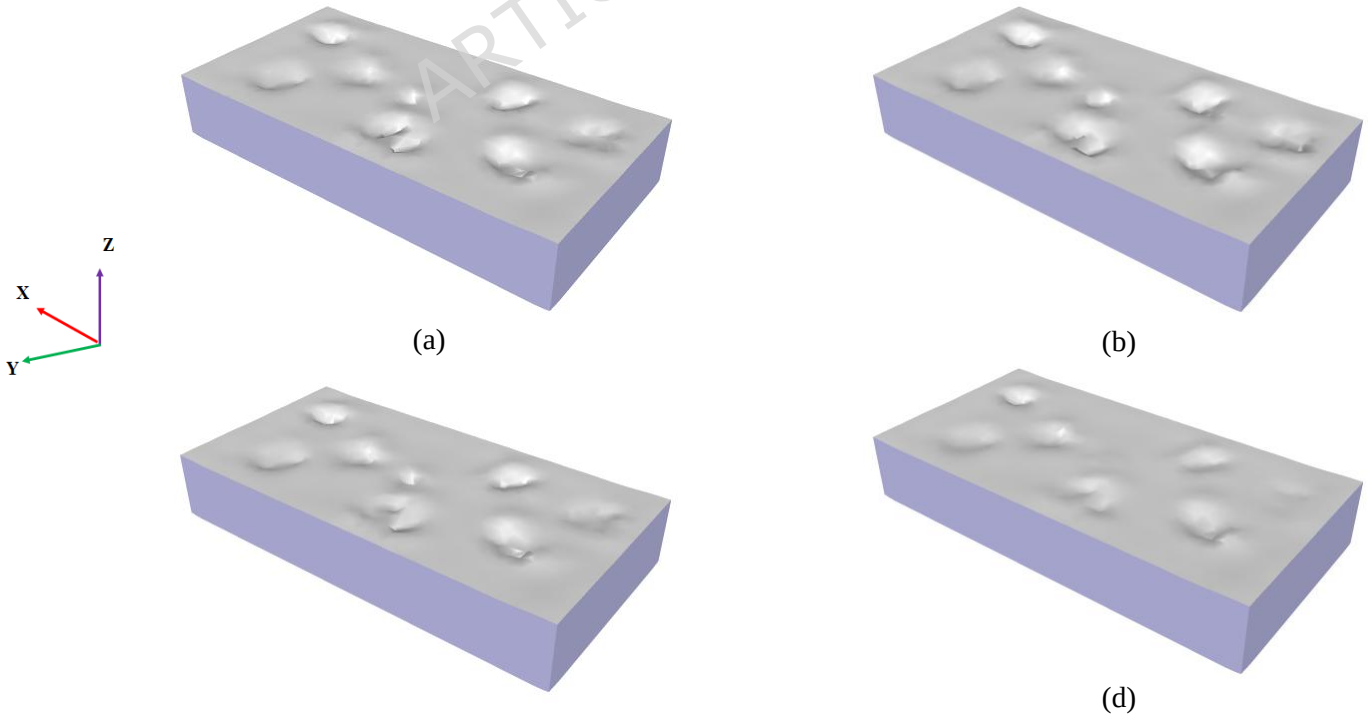

(a) (b)

(d)

(c)

Fig. 8. Atomic configurations obtained at different abrasive grain spacings: (a) 31 Å, (b) 35 Å, (c) 40 Å, and (d) 45 Å. The spacing is defined as the center-to-center distance between adjacent abrasive grains projected onto the silicon surface.

In the present MD analysis, detached atoms were defined as silicon atoms displaced from the substrate into a predefined material-removal region during grinding. Specifically, a dynamic group was used to count silicon atoms above the spatial threshold for the chip-removal zone. Accordingly, the number of detached atoms was determined as the instantaneous number of silicon atoms satisfying this geometric criterion during the final grinding stage. This definition provides a reproducible measure of material removal based on the atomic positions throughout the simulation. The variation in detached atoms can be interpreted through a coupled contact-mechanics and microstructural-evolution framework that incorporates both grinding penetration depth and abrasive grain spacing. As shown in Fig. 9, increasing the penetration depth from 10 Å to 16 Å increased the number of detached atoms from 2231 to 2495, indicating a transition from localized surface deformation to more extensive subsurface damage. At greater penetration depths, the abrasive grains interacted with a larger volume of material, generating higher compressive and shear stresses beneath the contact region. The resulting stress concentration led to lattice distortion, defect accumulation, increased dislocation activity, and grinding-induced amorphization and structural disorder in the silicon substrate. These microstructural changes progressively reduced lattice stability and weakened local atomic bonding, thereby facilitating atom detachment and material removal. Therefore, the increase in detached atoms originated not only from the larger contact volume but also from the enhanced evolution of subsurface defects and structural degradation.

This interpretation was consistent with previous investigations of silicon grinding. Li et al. [13]

demonstrated that increasing penetration depth intensified local stress concentration and promoted defect formation, structural disorder, and subsurface damage during nanometric grinding of monocrystalline silicon. Similarly, Wang et al. [36] reviewed modeling and simulation studies of precision silicon machining and concluded that plastic deformation, defect evolution, and pressure-induced structural transformation were the primary mechanisms governing material removal and the development of subsurface damage. The depth-dependent increase in detached atoms observed in the present study followed the same mechanistic trend.

In contrast, increasing abrasive grain spacing from 31 Å to 45 Å reduced the number of detached atoms from 2231 to 2154, revealing an inverse relationship between inter-grain spacing and material removal. When abrasive grains were positioned close to one another, the stress fields generated beneath neighboring contacts overlap and interact, producing larger deformation zones and stronger lattice instability. The resulting stress-field superposition enhanced defect accumulation and atomic displacement, thereby facilitating material removal. As the spacing increased, neighboring stress fields became more isolated, and the extent of interaction between them decreased. Consequently, deformation became more localized beneath individual abrasive contacts, reducing subsurface damage and limiting atom detachment. The combined results indicated that penetration depth and abrasive grain spacing influenced material removal through competing mechanisms. Increasing penetration depth promotes stress localization and defect accumulation, whereas increasing abrasive spacing suppresses stress-field overlap and reduces collective deformation among neighboring abrasive contacts. This behavior demonstrated a counteracting effect between two geometric parameters, highlighting the importance of simultaneously considering penetration depth and abrasive spacing when evaluating material-removal mechanisms in multi-abrasive ultrasonic vibration-assisted grinding.

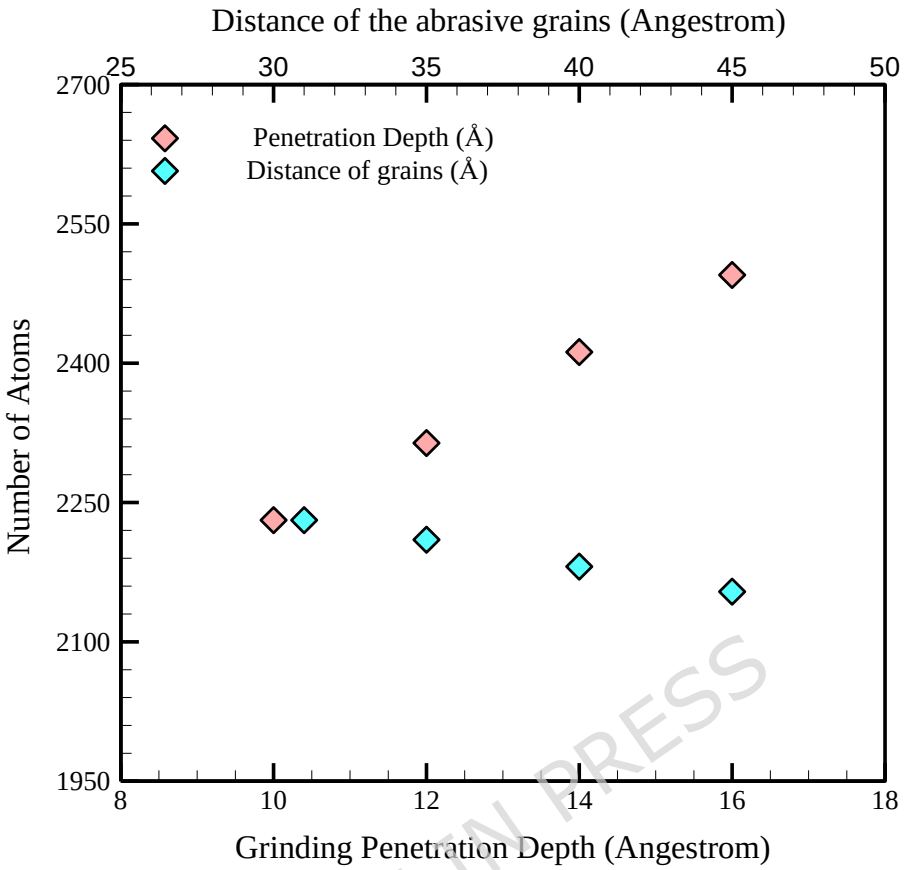

Fig.9. Effect of grinding penetration depth and abrasive grain spacing on the number of detached atoms during ultrasonic vibration-assisted grinding of monocrystalline silicon.

The atomic stress was evaluated using the LAMMPS compute stress/atom command, which outputs the per-atom virial stress tensor. During post-processing, each virial stress component was normalized by the corresponding atomic volume and subsequently converted into GPa. No spatial or temporal averaging was applied. Therefore, the reported maximum stress corresponds to the local atomic stress within the silicon substrate rather than the macroscopic continuum stress of the entire simulation box. By the abrasive process occurred in designed monocrystalline silicon, the stress distribution in this structure changed effectively as depicted in Fig. 10. The variation of maximum stress with grinding penetration depth and abrasive grain spacing is presented in Fig. 10. Increasing the penetration depth from 10 Å to 16 Å increased the maximum

stress from 10.26 GPa to 12.27 GPa, indicating progressively stronger stress concentration beneath the abrasive-workpiece contact zone. As the penetration depth increased, a larger volume of silicon was subjected to compressive and shear loading, resulting in greater lattice distortion and a broader deformation region. Elevated stress promoted defect accumulation, dislocation activity, and local structural disorder in the subsurface layer. Consequently, the deformation mechanism gradually evolved from localized near-surface deformation toward more extensive subsurface damage. The maximum stress obtained at the largest penetration depth (~12.27 GPa) was comparable to stress levels previously associated with crack initiation and severe grinding-induced damage in silicon. Zhang et al. [18] reported that increasing contact severity during single-grain grinding intensified subsurface stress concentration and promoted crack evolution within the silicon substrate. The present results followed a similar trend, indicating that deeper abrasive penetration substantially increased the mechanical driving force responsible for defect generation and material removal.

In contrast, increasing abrasive grain spacing from 31 Å to 45 Å reduced the maximum stress from 10.26 GPa to 9.89 GPa (Fig. 11), demonstrating that interactions among neighboring abrasive contacts strongly influenced stress evolution. At smaller spacing values, adjacent stress fields overlapped and reinforced one another, producing larger regions of concentrated stress beneath the grinding zone. This stress-field superposition enhanced lattice instability and promoted greater subsurface deformation. As the spacing increased, the deformation zones became increasingly isolated, and the interaction among neighboring stress fields decreased. Consequently, stress concentration became more localized beneath individual abrasive grains and the overall maximum stress within the substrate reduced. These observations indicated that maximum stress was governed not only by the severity of individual abrasive penetrations but

also by the collective interactions among neighboring abrasive grains. Increasing penetration depth intensified stress localization, whereas increasing abrasive spacing suppressed stress-field overlap. Therefore, the observed stress response showed the competing influence of contact severity and inter-grain interaction during multi-abrasive ultrasonic vibration-assisted grinding.

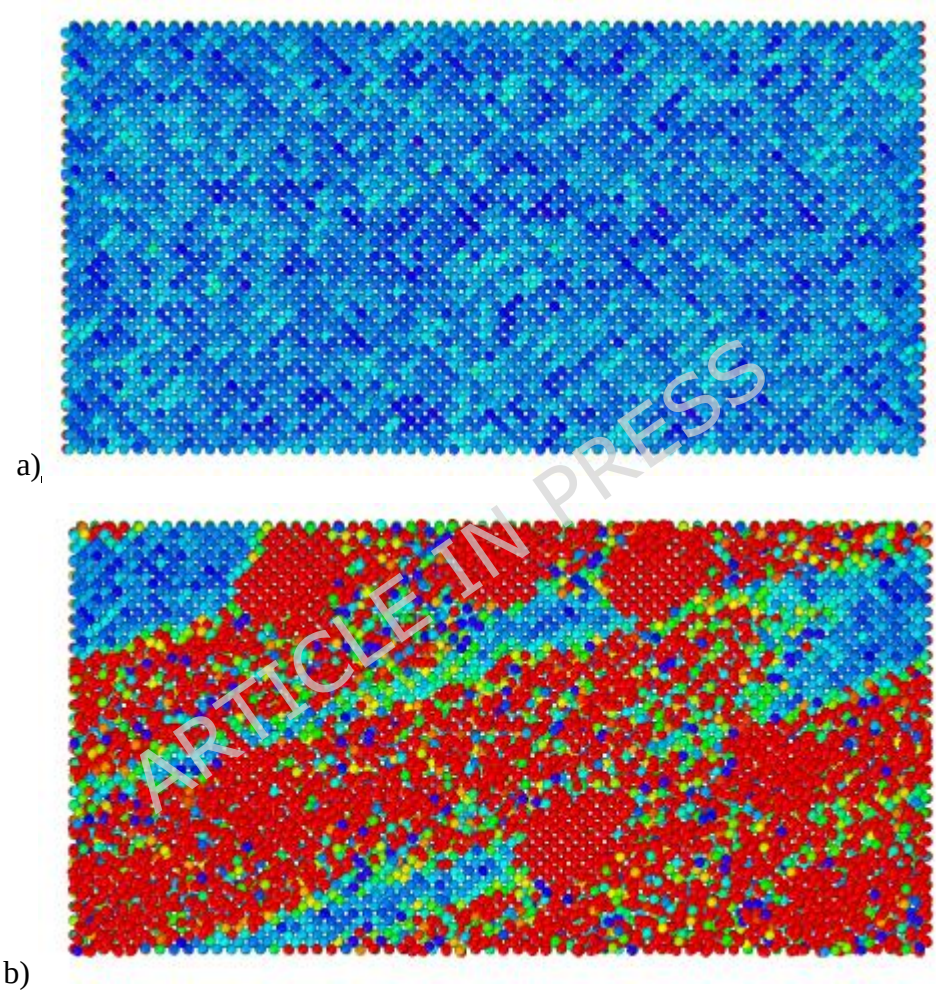

Fig.10. The stress distribution on the silicon substrate in the pristine modeled sample, a) before and b) after the abrasive process occurs.

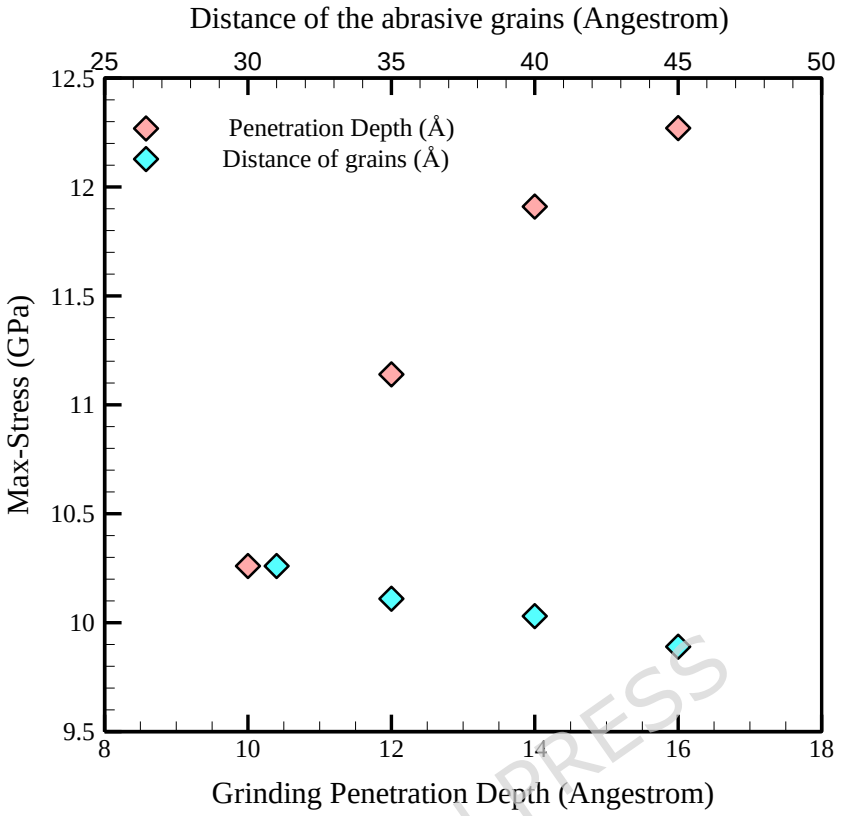

Fig.11. Effect of grinding penetration depth and abrasive grain spacing on the maximum von Mises stress developed within the silicon substrate during ultrasonic vibration-assisted grinding.

The variation in dislocation length provided additional insight into the microstructural response of the silicon substrate during grinding. As shown in Fig. 12, increasing the penetration depth from 10 Å to 16 Å increased the total dislocation length from 25.99 Å to 32.25 Å, indicating progressively greater defect accumulation and dislocation activity within the subsurface region. The greater penetration depth increased the volume of material subjected to severe compressive and shear loading, leading to more extensive lattice distortion and defect formation. Consequently, the dislocation network expanded with increasing penetration depth, demonstrating that deeper abrasive engagement promotes the evolution of irreversible plastic deformation within the silicon substrate. The increase in dislocation length was consistent with the simultaneous increases observed in detached atoms and maximum stress. Higher local

stresses facilitate lattice instability and structural disorder, which, in turn, promote the formation and growth of defect-rich regions beneath the abrasive contact zone. Therefore, the observed increase in dislocation length provided microstructural evidence that the material-removal process became increasingly governed by defect-mediated deformation mechanisms at larger penetration depths.

In contrast, increasing abrasive grain spacing from 31 Å to 45 Å reduced the dislocation length from 25.99 Å to 23.11 Å. This behavior indicated that the interaction among neighboring abrasive-induced stress fields played a critical role in defect evolution. At smaller spacing values, adjacent stress fields overlapped and reinforced each other, producing larger deformation zones and enhancing defect accumulation in the substrate. As the spacing increases, the degree of stress-field superposition decreases, resulting in more localized deformation beneath individual abrasive contacts. The reduction in collective deformation consequently limited the growth of defect-rich regions and suppressed the expansion of the dislocation network. These observations demonstrated that the combined influence of penetration depth and abrasive grain spacing governed dislocation evolution. Increasing penetration depth promoted defect accumulation and plastic deformation, whereas increasing abrasive spacing reduced stress-field interaction and limited defect development. The resulting trends established a direct microstructural link between geometric grinding parameters, stress evolution, and subsurface damage formation during multi-abrasive ultrasonic vibration-assisted grinding.

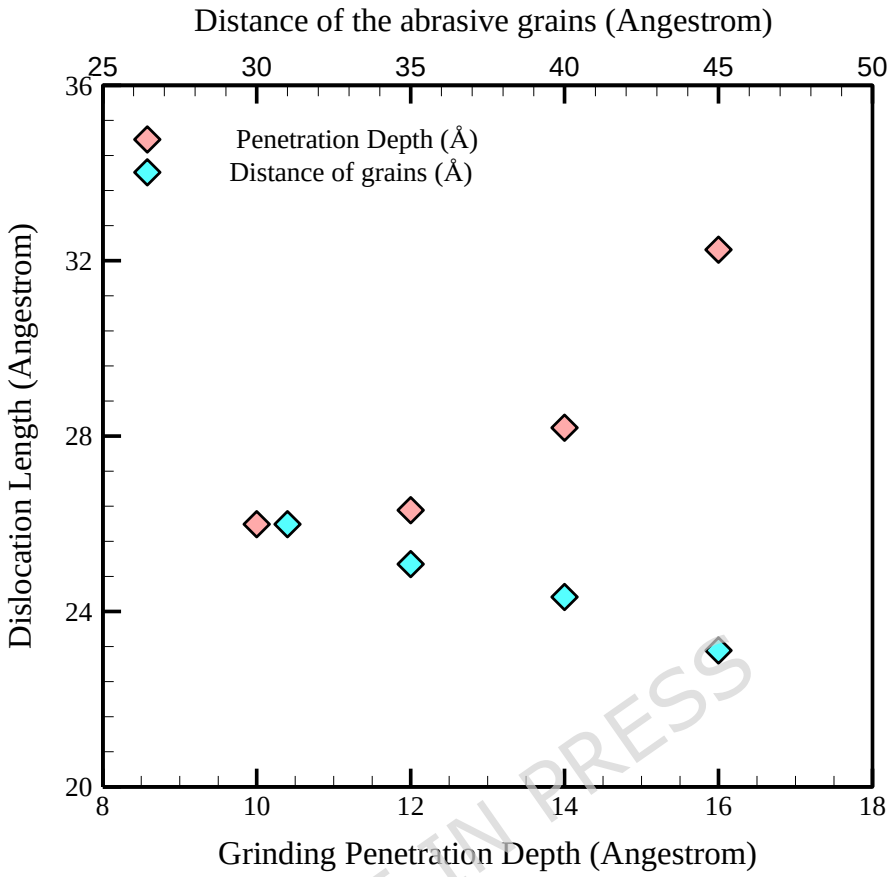

Fig.12. Effect of grinding penetration depth and abrasive grain spacing on the total dislocation length within the silicon substrate during ultrasonic vibration-assisted grinding.

The variation of maximum force with grinding penetration depth and abrasive grain spacing is presented in Fig. 13. Increasing the penetration depth from 10 Å to 16 Å increased the maximum force from 606.67 to 725.05 GPa·nm², indicating progressively stronger resistance of the silicon substrate to abrasive penetration. As the abrasive grains penetrated deeper into the substrate, a larger volume of material was subjected to compressive and shear loading, thereby increasing mechanical resistance at the abrasive–workpiece interface. The increased force transfer promoted bond stretching, bond rupture, defect accumulation, and dislocation activity within the subsurface region. Consequently, the deformation mechanism gradually evolved from localized

surface deformation toward more extensive defect-mediated plastic deformation. The increase in maximum force was consistent with the simultaneous increases observed in detached atoms, maximum stress, and dislocation length. Higher contact forces generated larger stress concentrations beneath the abrasive trajectories, thereby accelerating lattice distortion and structural degradation. These observations indicated that the increase in force was directly associated with the progression of subsurface damage and the increasing difficulty of deforming the silicon lattice at larger penetration depths.

In contrast, increasing abrasive grain spacing from 31 Å to 45 Å reduced the maximum force from 606.67 to 584.80 GPa·nm². This behavior indicated that the interaction among neighboring abrasive contacts strongly influenced force evolution. At smaller spacing values, overlapping stress fields concentrated mechanical loading within localized regions, thereby increasing the peak force experienced by the substrate. As the spacing increased, neighboring deformation zones became more isolated, and the degree of stress-field superposition decreased. Consequently, mechanical loading was distributed more uniformly beneath individual abrasive contacts, reducing the overall maximum force and limiting subsurface deformation. These results demonstrated that maximum force was determined not only by penetration depth but also by the collective interactions among neighboring abrasive grains. Increasing penetration depth intensifies mechanical loading and promotes defect accumulation, whereas increasing abrasive spacing reduces stress-field overlap and weakens collective deformation. Therefore, the force response showed the combined influence of contact severity and inter-grain interaction during multi-abrasive ultrasonic vibration-assisted grinding.

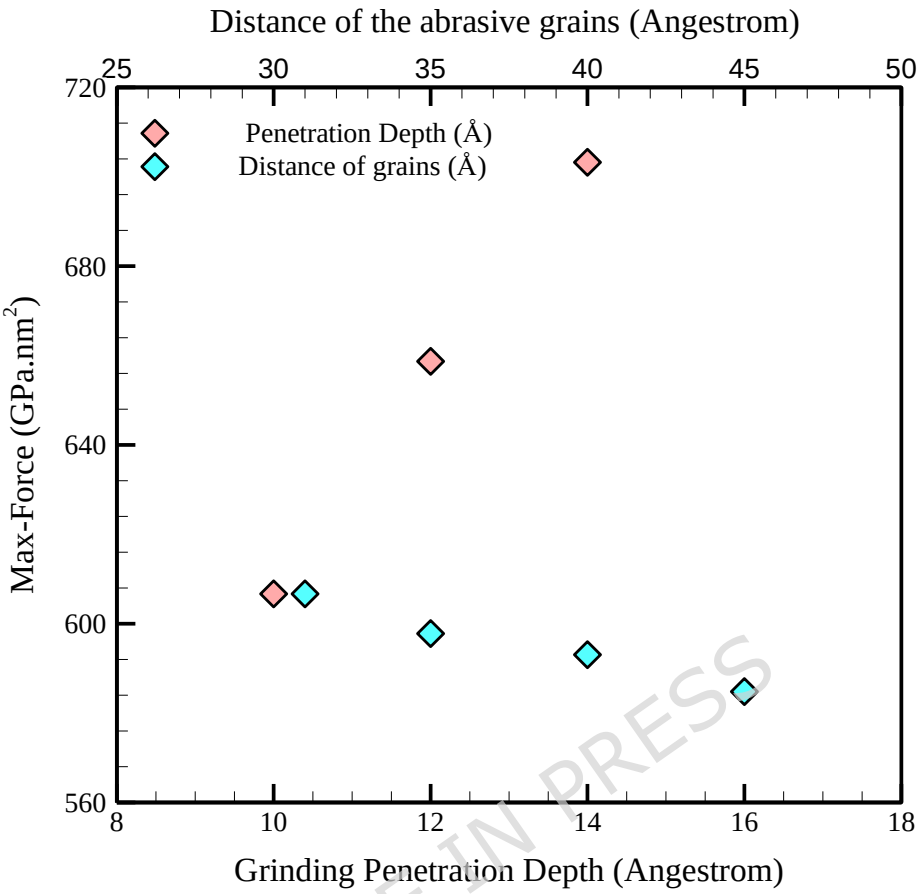

Fig.13. Effect of grinding penetration depth and abrasive grain spacing on the maximum force developed within the silicon substrate during ultrasonic vibration-assisted grinding.

The abrasive-substrate interaction energy was calculated using the LAMMPS compute group/group command, which evaluates the interaction energy between the abrasive-grain group and the silicon-substrate group. In the present study, the interaction energy is the energetic contribution from atomic interactions between abrasive grains and the silicon substrate during penetration and sliding. A more negative interaction energy indicates stronger energetic attraction between the two groups, whereas an increase toward less negative values reflects progressive bond deformation, atom detachment, and structural disruption during material removal. The interaction energy provides insight into the energetic state of the abrasive–workpiece interface and the degree of atomic interaction during grinding. As shown in Fig. 14,

increasing the penetration depth from 10 Å to 16 Å changed the interaction energy from approximately −0.67 eV to −0.51 eV. The progressive increase in interaction energy indicated a stronger mechanical interaction between the abrasive grains and the silicon substrate as the penetration depth increased. At greater penetration depths, more silicon atoms participate in the contact process, leading to greater bond deformation and increased energy transfer into the subsurface region. The increase in interaction energy was consistent with the simultaneous increases observed in maximum stress, dislocation length, and detached atoms. Higher interaction energies showed stronger abrasive–workpiece coupling, which promoted lattice distortion, defect accumulation, and structural disorder within the silicon substrate. Consequently, larger penetration depths facilitated the development of subsurface damage and increased the probability of atomic detachment. Therefore, the observed variation in interaction energy provides energetic evidence supporting the stress-driven and defect-mediated material-removal mechanisms discussed previously.

In contrast, increasing abrasive grain spacing from 31 Å to 45 Å reduced the interaction energy from approximately −0.67 eV to −0.81 eV. This behavior indicated that the interaction among neighboring abrasive-induced deformation zones became progressively weaker as the spacing increased. At smaller spacing values, overlapping stress fields intensified the local mechanical interaction between the abrasives and the substrate, leading to higher interaction energies and stronger lattice disturbance. As the spacing increased, stress-field overlap decreased, and the deformation became increasingly localized beneath individual abrasive contacts. The resulting reduction in collective deformation decreased the energy transferred into the substrate and suppressed defect accumulation. These results demonstrated that interaction energy served as an effective energetic descriptor linking geometric grinding parameters to the underlying atomistic

deformation mechanisms. Increasing the penetration depth strengthened the abrasive–workpiece coupling and promoted subsurface damage, whereas increasing the abrasive grain spacing weakened stress-field interaction and reduced the energetic driving force for defect evolution and material removal.

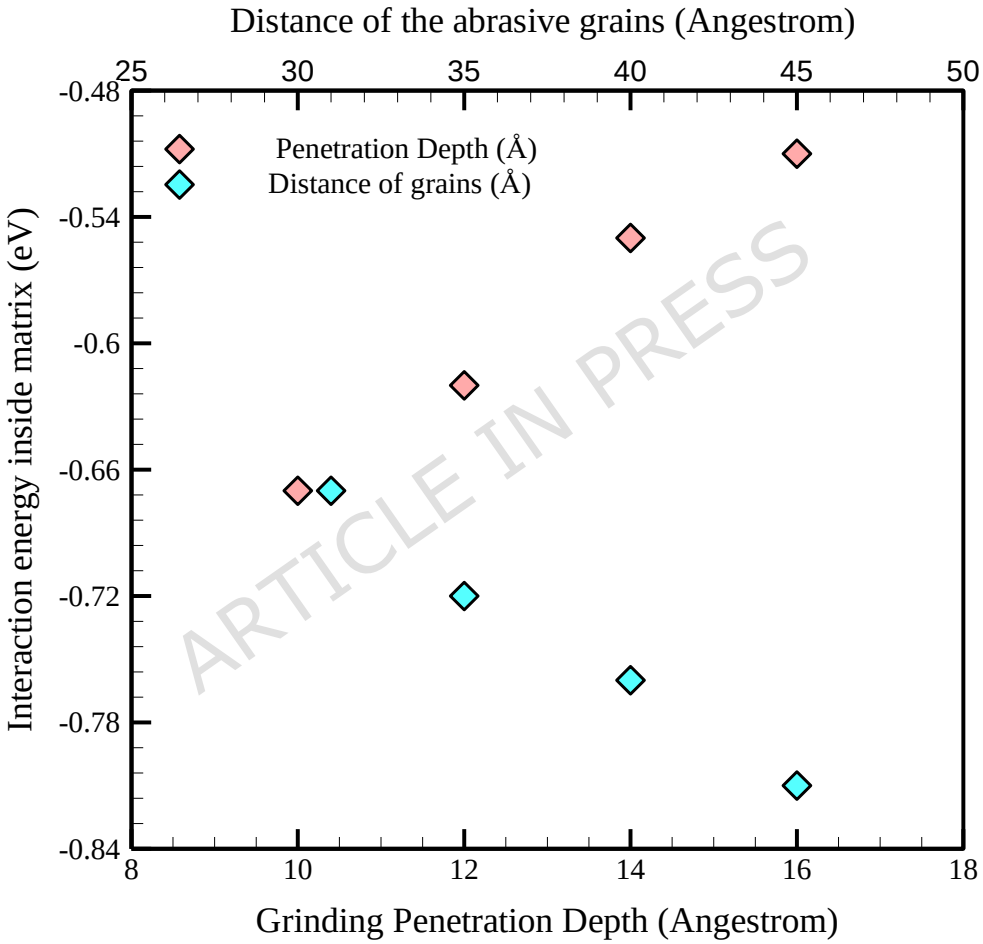

Fig.14. Effect of grinding penetration depth and abrasive grain spacing on the abrasive–workpiece interaction energy during ultrasonic vibration-assisted grinding of monocrystalline silicon.

Table 3 summarizes the effect of grinding penetration depth on the mechanical and structural response of the silicon substrate. Increasing the penetration depth from 10 Å to 16 Å produced a

systematic increase in detached atoms, maximum stress, maximum force, dislocation length, and interaction energy. Specifically, the number of detached atoms increased from 2231 to 2495, the maximum stress increased from 10.26 GPa to 12.27 GPa, and the dislocation length increased from 25.99 Å to 32.25 Å. The simultaneous increase in these quantities indicated that penetration depth governed material removal through a coupled stress–defect evolution mechanism. Larger penetration depths increased the contact volume between the abrasive grains and the substrate, thereby intensifying local stress concentration and promoting lattice distortion. The resulting structural instability facilitated defect accumulation and dislocation activity within the subsurface region, weakening local atomic bonding and promoting atom detachment. The increase in interaction energy further confirmed stronger abrasive–workpiece coupling and greater energy transfer into the silicon lattice at larger penetration depths. The consistent growth of stress, force, dislocation length, and detached atoms demonstrated that material removal became increasingly dominated by defect-mediated plastic deformation as the penetration depth increased. Therefore, penetration depth acted as a primary controlling parameter governing stress localization, subsurface damage evolution, and material removal during ultrasonic vibration-assisted grinding.

Table 3. Alterations in Physical Properties Resulting from Atomic Grinding of the Target Induced by Abrasive Grain Penetration Depth.

Grinding penetration depth (**Å**)	Number of separated atoms	Max-Stress (GPa)	Max-Force (GPa.nm^2)	Dislocation Length (Å)	Interaction energy inside matrix (eV)
10	2231	10.26	606.67	25.99	-0.67
12	2314	11.14	658.71	26.31	-0.62
14	2412	11.91	703.24	28.19	-0.55
16	2495	12.27	725.052	32.25	-0.51

The stress levels predicted in the present simulations were consistent with previously reported experimental and computational investigations of silicon deformation. Xuan et al. [35]

demonstrated that pressure-induced structural instability in silicon occurred within a well-defined stress range that depended on the loading condition and structural scale. Similarly, Fang et al. [20] reported that increasing cutting depth during atomic-scale machining promoted compressive stress accumulation and intensified subsurface structural damage. The observed increase in maximum stress from 10.26 GPa to 12.27 GPa therefore agreed with the established trend that increasing contact severity enhanced subsurface deformation and structural instability in silicon.

Table 4 summarizes the influence of abrasive grain spacing on the grinding response. Increasing the spacing from 31 Å to 45 Å resulted in a consistent reduction across all measured mechanical and structural indicators. The number of detached atoms decreased from 2231 to 2154, the maximum stress decreased from 10.26 GPa to 9.89 GPa, and the dislocation length decreased from 25.99 Å to 23.11 Å. These trends indicated that abrasive grain spacing controlled the degree of interaction among neighboring abrasive-induced stress fields. At small spacing values, overlapping deformation zones generated stronger stress-field superposition, thereby enhancing lattice instability, defect accumulation, and atomic detachment. As the spacing increased, neighboring stress fields became more isolated, reducing collective deformation and suppressing the development of subsurface damage. The simultaneous reduction in stress, force, interaction energy, dislocation length, and detached atoms demonstrated that abrasive grain spacing served as a regulatory parameter for stress-field interactions during multi-abrasive grinding. Larger spacing values reduced stress-field overlap and consequently limited the progression of defect-mediated material removal.

Table 4. Illustrates the variations in physical properties that occur due to the atomic grinding process of the target, correlated with the mean spacing of the abrasive grains.

The mean abrasive grain spacing of the abrasive	Number of separated atoms	Max-Stress (GPa)	Max-Force ($GPa.nm^2$)	Dislocation Length (Å)	Interaction energy inside matrix (eV)

grains (Å)					
31	2231	10.26	606.67	25.99	-0.67
35	2210	10.11	597.80	25.08	-0.72
40	2181	10.03	593.07	24.33	-0.76
45	2154	9.89	584.80	23.11	-0.81

Table 5 provides a direct comparison between the minimum and maximum combinations of grinding penetration depth and abrasive grain spacing. Although increasing penetration depth generally promoted stress localization, defect accumulation, and material removal, the simultaneous increase in abrasive grain spacing partially mitigated these effects by reducing the overlap of neighboring abrasive-induced stress fields. For example, the 45–16 Å condition exhibited lower detached atoms, maximum stress, maximum force, and dislocation length than would be expected if penetration depth alone governed the deformation process. This behavior suggests that the mechanical response of the silicon substrate should be interpreted by considering both geometric parameters together. It is important to note that the present simulations do not constitute a full factorial interaction analysis over the entire parameter space. Instead, the selected parameter combinations provide a mechanistic interpretation of how increased abrasive grain spacing can partially compensate for the enhanced deformation associated with deeper abrasive penetration. These observations indicate that the grinding penetration depth and abrasive grain spacing jointly influence material removal within the investigated parameter combinations and should therefore be considered simultaneously when optimizing ultrasonic vibration-assisted grinding.

Table 5. Alterations in physical properties resulting from atomic grinding of the target induced by MIN and MAX settings of abrasive grain penetration depth and mean abrasive grain spacing of the abrasive grains.

Abrasive grain spacing-Depth (Å)	Number of separated atoms	Max-Stress (GPa)	Max-Force (GPa.nm^2)	Dislocation Length (Å)	Interaction energy inside matrix (eV)
31-10 (MIN Values)	2231	10.26	606.67	25.99	-0.67
45-16 (MAX Values)	2203	10.18	602.15	25.72	-0.69

To further clarify the microstructural origin of observed mechanical behavior, cross-sectional atomic configurations before and after grinding are presented in Fig. 15. The pristine silicon substrate (Fig. 15a) exhibited a highly ordered crystalline arrangement with well-defined atomic layers and negligible structural disorder. Following ultrasonic vibration-assisted grinding (Fig. 15b), substantial modification of the near-surface region was observed. The abrasive–workpiece interaction produced localized lattice distortion, atomic displacement, and surface material removal, resulting in the formation of a damaged subsurface layer beneath the grinding zone. The crystallographic analysis shown in Fig. 15c provides additional evidence of structural evolution during grinding. Compared with the initially ordered crystal structure, the post-grinding configuration exhibited an expanded region of disordered atoms near the surface. This behavior indicated the accumulation of grinding-induced defects and local loss of crystalline order caused by repeated compressive and shear loading. The formation of these defect-rich regions was consistent with the observed increases in detached atoms, stress concentration, and interaction energy reported in the previous sections.

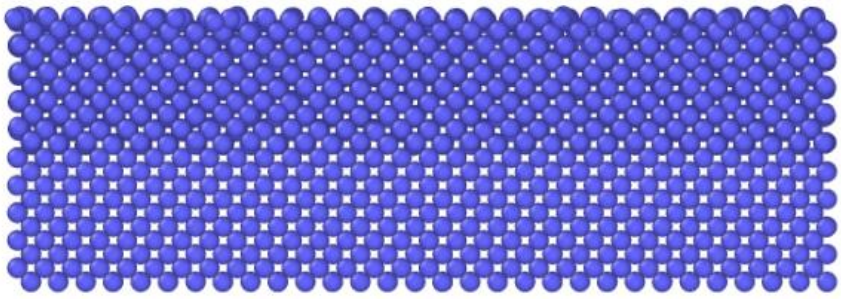

a)

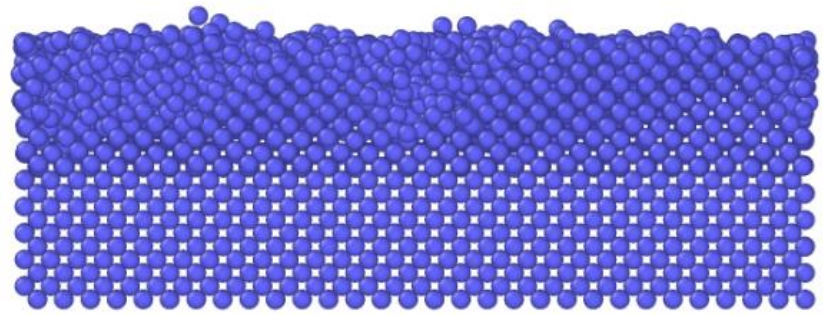

b)

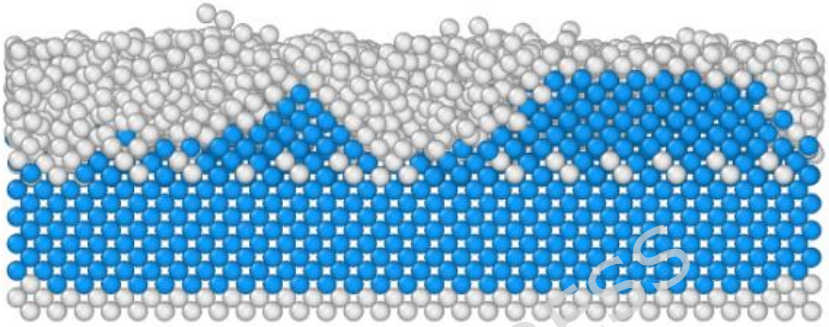

c)

Fig.15. Cross-sectional atomic configurations of the silicon substrate: (a) pristine crystal structure before grinding, (b) substrate after ultrasonic vibration-assisted grinding, and (c) crystallographic characterization showing the evolution of crystalline and defect-rich regions within the subsurface layer.

To quantify the defect evolution, the Dislocation Extraction Algorithm (DXA) implemented in OVITO was employed. A representative dislocation configuration is presented in Fig. 16a. The extracted dislocation lines indicate that grinding-induced deformation was accommodated not only by surface atom removal but also by subsurface defect development. The formation of dislocation networks provided a mechanism for stress relaxation within the silicon substrate and served as a direct indicator of plastic deformation at the atomic scale. The quantitative variation of dislocation length is shown in Fig. 16b. Increasing the penetration depth from 10 Å to 16 Å increased the dislocation length from approximately 65 Å to 88 Å, whereas increasing abrasive grain spacing from 31 Å to 45 Å reduced the dislocation length from approximately 65 Å to 49 Å. These trends demonstrated that deeper penetration promoted greater lattice distortion and

defect accumulation, while larger abrasive spacing reduced the overlap of neighboring stress fields and suppressed defect development. Consequently, the evolution of dislocation length provided direct microstructural evidence supporting previously observed trends in stress, force, interaction energy, and atom detachment. The combined observations from Figs. 15 and 16 established a clear mechanistic relationship between geometric grinding parameters and material-removal behavior. Increasing penetration depth intensified subsurface deformation and defect accumulation, whereas increasing abrasive grain spacing limited stress-field interaction and suppressed defect evolution. Therefore, the material-removal process during ultrasonic vibration-assisted grinding was governed by the coupled evolution of stress concentration, lattice disorder, and dislocation-mediated deformation within the silicon substrate

a)

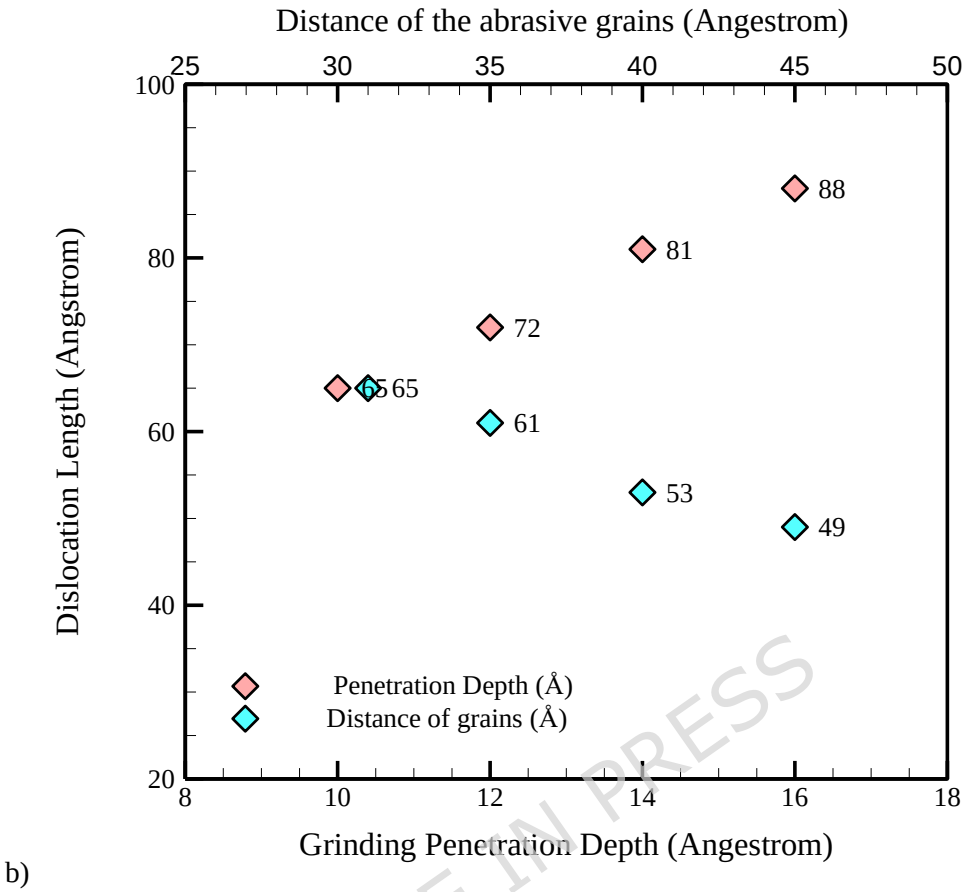

b)

Fig.16. Representative dislocation structure extracted using the Dislocation Extraction Algorithm (DXA) after grinding and (b) effect of grinding penetration depth and abrasive grain spacing on the total dislocation length within the silicon substrate.

3.4. Summary of Findings

The present molecular dynamics simulations demonstrated that the grinding behavior of monocrystalline silicon was governed by the coupled influence of grinding penetration depth and abrasive grain spacing. Increasing the penetration depth from 10 Å to 16 Å systematically increased the number of detached atoms, the maximum stress, the maximum force, the dislocation length, and the abrasive–workpiece interaction energy. Cross-sectional structural analysis and DXA characterization revealed that these changes were accompanied by enhanced

lattice distortion, defect accumulation, and the development of subsurface damage, indicating a transition toward more pronounced defect-mediated plastic deformation at greater penetration depths. In contrast, increasing abrasive grain spacing from 31 Å to 45 Å reduced detached atoms, stress, force, interaction energy, and dislocation length. This behavior was attributed to the progressive reduction of stress-field overlap among neighboring abrasive grains. Larger spacing values localized deformation beneath individual contacts and suppressed collective subsurface damage evolution, resulting in lower defect accumulation and reduced material removal.

The combined analysis of atomic configurations, stress evolution, interaction energy, and dislocation development established a direct mechanistic relationship between geometric grinding parameters and material-removal behavior. The results indicate that penetration depth primarily controlled contact severity and defect generation, whereas abrasive grain spacing regulated stress-field interaction among neighboring abrasives. Therefore, material removal during ultrasonic vibration-assisted grinding was governed by the coupled evolution of stress concentration, lattice disorder, and dislocation-mediated deformation within the silicon substrate.

4. Conclusion

This study employed MD simulations to investigate the influence of grinding penetration depth and abrasive grain spacing on the deformation behavior of monocrystalline silicon during ultrasonic vibration-assisted grinding. Before grinding, the system was thermally equilibrated under controlled conditions, and the convergence of kinetic energy, total energy, temperature, RMSD, and RDF confirmed thermodynamic stability. The results demonstrated that grinding penetration depth and abrasive grain spacing exerted opposite effects on the grinding response. Increasing the penetration depth from 10 Å to 16 Å increased the number of detached atoms from 2231 to 2495, the maximum stress from 10.26 GPa to 12.27 GPa, the maximum force from

606.67 GPa·nm² to 725.05 GPa·nm², and the dislocation length from 25.99 Å to 32.25 Å. These changes indicated that deeper abrasive penetration intensified stress localization, defect accumulation, and the development of subsurface damage.

In contrast, increasing the abrasive grain spacing from 31 Å to 45 Å reduced the number of detached atoms from 2231 to 2154, the maximum stress from 10.26 GPa to 9.89 GPa, the maximum force from 606.67 GPa·nm² to 584.80 GPa·nm², and the dislocation length from 25.99 Å to 23.11 Å. The reduction was attributed to weaker interaction among neighboring abrasive-induced stress fields and diminished collective deformation. The combined analysis of atomic configurations, interaction energy, stress evolution, and dislocation development revealed that penetration depth primarily governed contact severity, whereas abrasive grain spacing controlled the extent of stress-field interaction among neighboring abrasives. Consequently, the material-removal behavior was found to be governed by the coupled evolution of stress concentration, lattice disorder, and defect-mediated deformation within the silicon substrate.

The present study was subject to several limitations. The abrasive grains were modeled as rigid bodies; abrasive wear was not considered, and the GHz-scale vibration served as an atomistic computational analog rather than a direct representation of industrial ultrasonic frequencies. In addition, the simulations were restricted to a single material system and nanoscale timescales. Future work should incorporate structural analyses, such as phase-identification methods, experimental validation, longer simulation durations, and additional material systems to improve further the physical interpretation and practical applicability of the proposed framework.

Declaration

Ethics approval and consent to participate: N/A

- **Consent for publication:** N/A
- **Competing interests:** N/A
- **Funding:** N/A
- **Authors' contributions:**

Narinderjit Singh Sawaran Singh Funding acquisition, simulation/model setup, Writing – review and editing

Waqed H. Hassan Formal analysis, Data curation,

Waleed Alaloosi Funding acquisition, Formal analysis, simulation/model setup

Watfaa Khayri Younis Writing – original draft; Writing – review and editing

Mahmut Taner Funding acquisition, Writing – review and editing simulation/model setup

Soheil Salahshour Writing – original draft; Writing – review and editing

S. Mohammad Sajadi: Funding acquisition, Formal analysis, Data curation, simulation/model setup

- **Acknowledgments:** N/A
- **Availability of data and material:** N/A

Data Availability Statement

The data that support the findings of this study are available from the corresponding author, upon reasonable request.

Funding Declaration: Not Applicable

References

[1] Z. Zhang, F. Xie, W. J. M. P. Wang, and E. M. Review, "Ultrasonic-assisted synthesis of lead citrate as precursor for preparation of lead oxide from lead sulfate", *Mineral Processing and Extractive Metallurgy Review,* vol. 47, no. 1, pp. 141-154, 2026.

[2] X. Bu, J. K. Danstan, A. Hassanzadeh, A. Behrad Vakylabad, S. Chelgani, and E. M. Review, "Metal extraction from ores and waste materials by ultrasound-assisted leaching-an overview", *Mineral Processing and Extractive Metallurgy Review,* vol. 45, no. 1, pp. 28-45, 2024.

[3] V. Singh, P. Dixit, R. Venugopal, K. Venkatesh, and E. M. Review, "Ore pretreatment methods for grinding: Journey and prospects", *Mineral Processing and Extractive Metallurgy Review,* vol. 40, no. 1, pp. 1-15, 2019.

[4] M. Marques *et al.*, "Exploring the challenges and advances in concentrating ultrafine iron ore particles with a focus on goethite", *Mineral Processing and Extractive Metallurgy Review*, vol. 46, no. 2, pp. 254-267, 2025.

[5] A. Kumar, R. Sahu, and S. Tripathy, "Energy-efficient advanced ultrafine grinding of particles using stirred mills—a review" , *Energies*, vol. 16, no. 14, p. 5277, 2023.

[6] C. Liu *et al.*, "A review of ultrasonic vibration-assisted grinding for advanced materials" , *Intelligent and Sustainable Manufacturing,* vol. 2, no. 1, p. 10001, 2025.

[7] J. Jin, J. Mao, R. Wang, and M. J. M. Cui, "Experimental Study on Ultrasonic Vibration-Assisted Grinding of SiCp/Al Composites Grinding", *Micromachines,* vol. 16, no. 3, p. 302, 2025.

[8] Y. Cao *et al.*, "Evaluation of Ultrasonic Vibration-Assisted Grinding in Multi-Process Profile Grinding of K4002 Nickel-Based Superalloy Blade Tenons" , *Materials*, vol. 18, no. 7, p. 1437, 2025.

[9] D. Wang, H. Fan, D. Xu, and Y. J. A. S. Zhang, "Research on grinding force of ultrasonic vibration-assisted grinding of C/SiC composite materials", *Applied Sciences,* vol. 12, no. 20, p. 10352, 2022.

[10] Y. Liu, Y. Ji, L. Dong, H. Xie, J. Song, and J. A. Li, "Effect of grinding depths on SiC nanogrinding behavior based on molecular dynamics", *Applied Physics A,* vol. 128, no. 1, p. 34, 2022.

[11] Z. Li *et al.*, "Molecular dynamics study on burr formation mechanism during monocrystalline silicon nano-grinding process", *Journal of Manufacturing Processes,* vol. 131, pp. 2505-2513, 2024.

[12] L. J. A. P. A. Chen, "Effect of humidity on grinding force of TiAl alloy at nanometer scale", *Applied Physics A,* vol. 130, no. 4, p. 234, 2024.

[13] M. Li, D. Chang, P. Zhao, and J. J. M. Tan, "Molecular Dynamics Study on the Effect of Surface Films on the Nanometric Grinding Mechanism of Single-Crystal Silicon", *Micromachines,* vol. 16, no. 10, p. 1141, 2025.

[14] Y. Huang, Y. Zhou, J. Li, F. Zhu, and R. Materials, "Understanding of the effect of wear particles removal from the surface on grinding silicon carbide by molecular dynamics simulations", *Diamond and Related Materials,* vol. 137, p. 110150, 2023.

[15] B. Wu, Y. Sun, and S. J. T. L. Wu, "Molecular dynamics study of nano-grinding behavior for silicon wafer workpieces with nanoscale roughness under diamond abrasive rotation and translation", *Tribology Letters,* vol. 72, no. 1, p. 26, 2024.

[16] P. Zhao, B. Zhao, J. Pan, and J. Wu, "Nano-grinding process of single-crystal silicon using molecular dynamics simulation: Nano-grinding parameters effect" , *Materials Science in Semiconductor Processing*, vol. 143, p. 106531, 2022.

[17] S. Li *et al.*, "Molecular dynamics simulation of the material removal characteristics for monocrystalline silicon: A comparative study of various cutting methods", *Journal of Mechanical Science and Technology,* vol. 39, no. 10, pp. 5925-5938, 2025.

[18] Z. Zhang *et al.*, "Origin and evolution of a crack in silicon induced by a single grain grinding" , *Journal of Manufacturing Processes*, vol. 75, pp. 617-626, 2022.
[19] M. Li *et al.*, "Effect of grinding damage on cutting force and ductile machining during single grain scratching of monocrystalline silicon", *Materials Science in Semiconductor Processing*, vol. 151, p. 107019, 2022.
[20] X. Fang, Q. Kang, J. Ding, L. Sun, R. Maeda, and Z. J. M. Jiang, "Stress distribution in silicon subjected to atomic scale grinding with a curved tool path" , *Materials*, vol. 13, no. 7, p. 1710, 2020.
[21] W. Huang, J. Tang, W. Zhou, J. Wen, and M. J. Yi, "Molecular dynamics simulations of ultrasonic vibration-assisted grinding of polycrystalline iron: nanoscale plastic deformation mechanism and microstructural evolution", *Applied Surface Science*, vol. 640, p. 158440, 2023.
[22] N. E. Karkalos and A. P. J. M. Markopoulos, "Molecular dynamics study of the effect of abrasive grains orientation and spacing during nanogrinding", *Micromachines*, vol. 11, no. 8, p. 712, 2020.
[23] J. Tersoff, "New empirical approach for the structure and energy of covalent systems", *Physical Review B*, vol. 37, no. 12, p. 6991, 1988.
[24] A. Mosavi, M. Hekmatifar, A. a. Alizadeh, D. Toghraie, R. Sabetvand, and A. Karimipour, " The molecular dynamics simulation of thermal manner of Ar/Cu nanofluid flow: The effects of spherical barriers size", *Journal of Molecular Liquids*, vol.319, 2020.
[25] S. Sun *et al.*, "Examination of the mechanical properties of porous carbon matrix by considering the Nanovoids: A computational study using molecular dynamics simulation", *International Communications in Heat and Mass Transfer*, vol. 160, p. 108399, 2025.
[26] S. Liu *et al.*, "Numerical study of changes in the mechanical and thermal property of porous silicon sample with increasing initial temperature: A molecular dynamics approach", *International Communications in Heat and Mass Transfer*, vol. 159, p. 108339, 2024.
[27] N. S. S. Singh *et al.*, "Effect of copper nanoparticle volume fraction on flow in a 3D lid-driven cavity with phase change materials using molecular dynamics simulation", *Case Studies in Chemical and Environmental Engineering*, vol. 11, p. 101181, 2025.
[28] X. Li *et al.*, "The impact of channel edge type on the particle diffusion and permeability of carbon nanotubes as a membrane in reverse electrodialysis process using molecular dynamics simulation" , *International Communications in Heat and Mass Transfer*, vol. 164, p. 108930, 2025.
[29] Y. Liu *et al.*, "Molecular dynamics simulation of thermal behavior of paraffin/Cu nanoparticle PCM in a non-connected rotating ribbed tube", *International Communications in Heat and Mass Transfer*, vol. 165, p. 109058, 2025.
[30] H. Wang *et al.*, "Thermal and mechanical attributes and swelling percentage of hydrogels by changing in magnetic field frequency using computer simulation" , *International Communications in Heat and Mass Transfer*, vol. 165, p. 109070, 2025.
[31] N. S. S. Singh, A. B. Ali, H. F. M. Ameen, A. S. Fahem, S. Salahshour, and S. Eftekhari, "Effect of atomic porosity on the mechanical properties of aluminium polycrystalline using molecular dynamics simulation" , *Results in Engineering*, vol. 25, p. 104491, 2025.
[32] Z. Yang, T. Yu, and G. J. L. Wang, "Molecular Dynamics Simulation of Single-Crystal Silicon CMP Using Ultrasonic Vibration-Assisted and Hollow Silica Abrasives", *Langmuir*, vol.42, 2026.
[33] C. Yang, Y. Wang, X. Xu, and m. transfer, "Molecular dynamics studies of ultrafast laser-induced phase and structural change in crystalline silicon", *International Journal of Heat and Mass Transfer*, vol. 55, no. 21-22, pp. 6060-6066, 2012.
[34] K. J. M. P. Persson, "Materials data on Si (SG: 227) by materials project" , *Mater. Proj*, vol. 10, p. 1191632, 2014.
[35] Y. Xuan *et al.*, "Pressure-induced phase transitions in nanostructured silicon", *The Journal of Physical Chemistry C*, vol. 124, no. 49, pp. 27089-27096, 2020.
[36] H. Wang, M. Bai, Y. Wu, J. Du, Y. Zhang, and W. Ming, "A systematic review of precision

mechanical machining processes for monocrystalline silicon based on modeling and simulation" , *The International Journal of Advanced Manufacturing Technology,* vol. 136, no. 11, pp. 4715-4749, 2025.